Supporting Information:

Chiral Au(III) chelates exhibit unique NCI-60 cytotoxicity profiles and interactions with human serum albumin

Sheldon Sookai,*[,a] Matthew P. Akerman[b] and Orde Q. Munro*[,a,c]

[a]*Molecular Sciences Institute, School of Chemistry, University of the Witwatersrand, PO WITS 2050, Johannesburg, South Africa*

[b]*School of Chemistry and Physics, University of KwaZulu-Natal, Pietermaritzburg, 3201, South Africa*

[c]*School of Chemistry, University of Leeds, Woodhouse Lane, Leeds, LS2 9JT, UK*

E-mail: Sheldon.Sookai@wits.ac.za

O.Munro@leeds.ac.uk

Akermanm@ukzn.ac.za

Table of Contents

1. Experimental Methods

All solvents (HPLC grade) and chemical synthons were used as received from Merck Sigma-Aldrich® without further purification. Deuterated dimethyl sulfoxide was stored over activated 4 Å molecular sieves. Human serum albumin (HSA) was purchased from Sigma and used as received without further purification. Ultrapure water (Type I) was produced using a Merk-Millipore Direct-Q® 3 UV Water Purification System.

1.1 Instruments

1.1.1. Crystallography

The single crystal X-ray structure determination for **AuL1** was carried out with a three-circle Bruker Apex-II X-ray diffractometer equipped with a CCD area detector and a fine-focus sealed X-ray tube source (Mo anode). The crystal was mounted under Paratone® oil on a nylon loop (Hampton Research) and the crystal was kept at 173(1) K during data collection (Oxford CryoStream 700). Using Olex2,[1] the structure was solved with the ShelXT[2] structure solution program (intrinsic phasing) and refined with ShelXL[3] using least squares minimization.

The single crystal X-ray structure determination for **AuL2** was carried out with a four-circle Oxford Xcalibur2 X-ray diffractometer equipped with a CCD area detector and a fine-focus sealed X-ray tube source (Mo anode). The crystal was affixed upon a glass microfibre with epoxy cement for data collection and the crystal was kept at 100(2) K during data collection (Oxford CryoStream 700). The structure was solved and refined as above using

least squares minimization. Thereafter, the structure was further refined using Olex2 by implementing aspherical atomic form factors in the module NoSpherA2[4] interfaced with Orca 5.0.3.[5,6] The wavefunction for the system was determined at the PBE[7]/Jorge-DZP-DKH level of theory (relativistic Hamiltonian and basis set).[8]

1.1.2. General spectroscopy

Nuclear magnetic resonance (NMR) spectra were recorded on either a Bruker Avance III 400 (400.21 MHz for ^{1}H, 100.64 MHz for ^{13}C, 162.01 MHz for ^{31}P and 376.57 MHz for ^{19}F) or a Bruker Avance-III-300 spectrometer operating at 300.13 MHz for ^{1}H, 75.47 MHz for ^{13}C, 121.49 MHz for ^{31}P and 282.40 MHz for ^{19}F. All spectra were recorded at 298 K with 5 mm BBOZ or TBIZ probes. Deuterated solvent signals were used to correct for the reported chemical shifts in δ (in ppm). For $(CD_3)_2SO$, $CDCl_3$, D_2O and CD_3OD the δ H was referenced as 2.50, 7.26, 4.79 and 3.31 ppm, respectively, and the δ ^{13}C {^{1}H} was referenced at 39.52, 77.16, D_2O had no peak, and 49 ppm, respectively. MestReNova (version 14.2.1-27684) was used to analyse NMR spectra. The coupling patterns are abbreviated as follows: s - singlet; d - double; t - triplet; q - quartet; sept – septet; m – multiplet; br s – broad signal. Proton coupling constants (J) are given in hertz (Hz). Impurities are stated on the NMR figures.[9] FT-IR spectra of powder samples were recorded using a Bruker Alpha FTIR spectrometer incorporating a Bruker Platinum® diamond ATR sampling accessory. Spectra were analysed using the OPUS software package on the spectrometer (version 7.5). Mass spectra were recorded with a Bruker Compact Q-TOF high-resolution mass spectrometer using Bruker Daltronics HyStar 3.2 SR4 software. Bruker Compass DataAnalysis software (Version 4.3) was used to analyse chromatograms. Samples of pure compounds (typically ca. 10 µg/mL) were prepared in HPLC grade acetonitrile or methanol for metal chelates and HPLC grade methanol for ligands. Solutions were acidified using 0.1% (V/V) formic acid. UV-Vis electronic spectra were recorded using either a PerkinElmer Lambda 365 double beam spectrometer connected to a Peltier controller and multicell thermostatic cell block or an Analytik Jena Specord210 Plus double-beam instrument fitted with an external water circulating thermostatic bath and thermostatted cell holders. The spectral data were analysed with the spectrometer software or Origin Pro 2020. Spectra were recorded (10-mm pathlength quartz cuvettes) as a function of concentration for both characterisation and the determination of molar absorptivity constants.

1.2 Compound Synthesis

1.2.1. Synthesis of enantiomerically pure ligands

(1*S*,2*S*) and (1*R*,2*R*)-*N*,*N*'-bis[(1*E*)-1*H*-pyrrol-2-ylmethylene] cyclohexane -1,2-diamine (**H_2L1** and **H_2L2**). Both enantiomerically pure ligands were synthesized by grinding the enantiomerically pure (1*S*, 2*S*)- or (1*R*, 2*R*)-cyclohexane diamine (0.303 g, 2.65 mmol) with an agate pestle and mortar with pyrrole-2-carboxaldehyde (0.500 g, 5.30 mmol) for between 10 to 15 minutes, until a brown oil was formed. The brown oil was dissolved in dichloromethane and dried with $MgSO_4$ to remove the water from the condensation reaction. The solution was filtered through celite before been layered with hexane, which yielded thin white rod-shaped crystals. A yield of 65% was obtained.

1.2.2. Synthesis of *tert*-butylammonium tetrachloroaurate(III)

Hydrogen tetrachloroaurate(III) (1.218 g) was dissolved in 50 ml of deionized water. The solution was then added to a solution of *tert*-butylammonium hydrogen sulphate (1.020 g) resulting in the formation of a bright yellow precipitate which was $[Bu_4N][AuCl_4]$ (lipophilic gold(III) salt). $[Bu_4N][AuCl_4]$ was extracted into chloroform, dried over $MgSO_4$ before been filtered and the chloroform was removed by rotary evaporation. The resulting material was a crystalline bright yellow powder (1.55 g, 88%).

$$H[AuCl_4]_{(aq)} + [Bu_4N][HSO_4]_{(s)} \longrightarrow [Bu_4N][AuCl_4]_{(s)} + H_2SO_{4\ (aq)}$$

1.2.3. Metalation of the enantiomerically pure ligands

The synthesis of 2,2'-{(1*S*,2*S*) or 2,2'-{(1*R*,2*R*)-cyclohexane-1,2-diylbis[nitrilo(*E*)methylylidene]}bis (pyrrol-1-ido)gold(III) hexafluorophosphate(V) [Au((1*S*,2*S*)**L1**)PF_6 (**AuL1**) and [Au((1*R*,2*R*)**L2**)]PF_6 (**AuL2**) occurs via the same procedure from the enantiopure ligands. To a 50 ml round bottom flask containing the pure solid ligand (201 mg, 0.750 mmol) was added 10 ml of ethanol, which was heated to dissolve the ligand. The solution was then allowed to cool to room temperature. Thereafter, a 10 ml solution of dry dichloromethane containing $[Bu_4N][PF_6]$ (133 mg, 0.344 mmol) and $[Bu_4N][AuCl_4]$ (100 mg, 0.172 mmol) was added. The solution was stirred for around 3 hours at ambient temperature until an orangish-yellow precipitate had formed. The precipitate was filtered and washed with dry dichloromethane. Red-orange crystals suitable for single crystal XRD were grown by vapour diffusion of diethyl ether into an acetonitrile solution of the product. The crystalline salts were shown to be **AuL1** and **AuL2** by X-ray crystallography.

1.2.4. Characterisation of the enantiomerically pure ligands

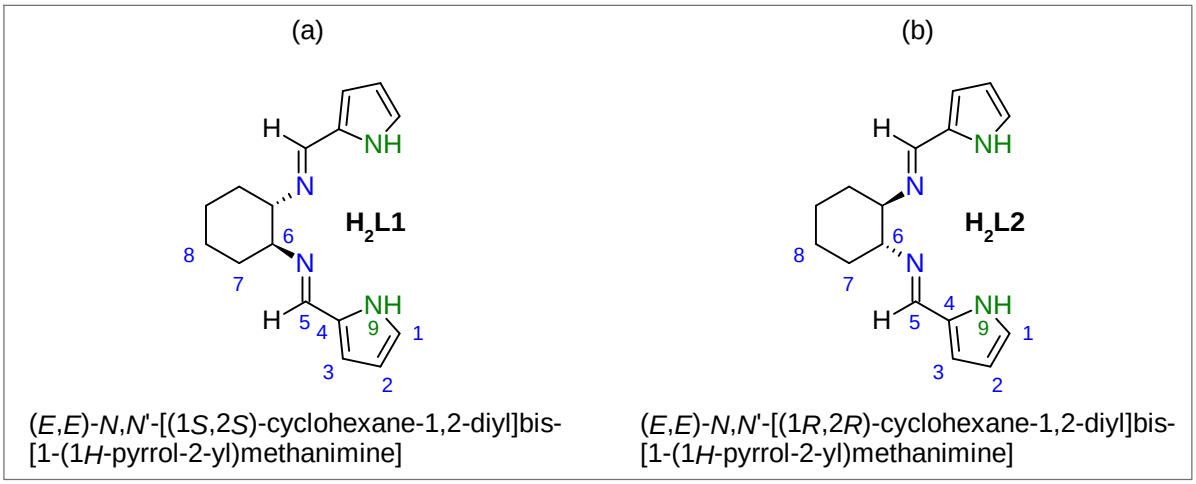

(*E*,*E*)-*N*,*N*'-[(1*S*,2*S*)-cyclohexane-1,2-diyl]bis-[1-(1*H*-pyrrol-2-yl)methanimine]

(*E*,*E*)-*N*,*N*'-[(1*R*,2*R*)-cyclohexane-1,2-diyl]bis-[1-(1*H*-pyrrol-2-yl)methanimine]

Scheme 1. Structures of (a) **H_2L1** and (b) **H_2L2** showing the atom numbering sequence.

IR (cm^{-1}): 3218w δ(NH, pyrrole), 3110m br δ(CH, imine), 2944 – 2853s ν(CH_2), 1627s ν(C=N). ^{1}H NMR (400 MHz, DMSO-d_6, 300 K) [δ, ppm]: 1.34 – 1.80 (m, 8H, H-7 and H-8), 3.23 (m, 2H, H-6), 6.01 (t, J = 3.0 Hz, 2H, H-2), 6.31(dd, $^3J_1$ = 3.5 Hz, $^3J_2$ 1.4 Hz, 2H, H-3), 6.76 (t, J = 1.9 Hz, 2H, H-1), 7.94 (s, 2H, H-5), 11.16 (s, 2H, H-9). ^{13}C NMR (101 MHz, DMSO-d_6, 298 K) [δ, ppm]: 24.70 (C-8), 33.85 (C-7), 74.09 (C-6), 109.07 (C-2), 113.61 (C-3), 122.08 (C-1),

130.33 (C-4), 151.26 (C-5). UV-vis (acetonitrile) [λ, max, nm; ε, mol^{-1} dm^3 cm^{-1}]: 289; 2.95 × 10^4 (**H_2L1**) and 2.37 x 10^4 (**H_2L2**).

1.2.5. Characterisation of AuL1 and AuL2

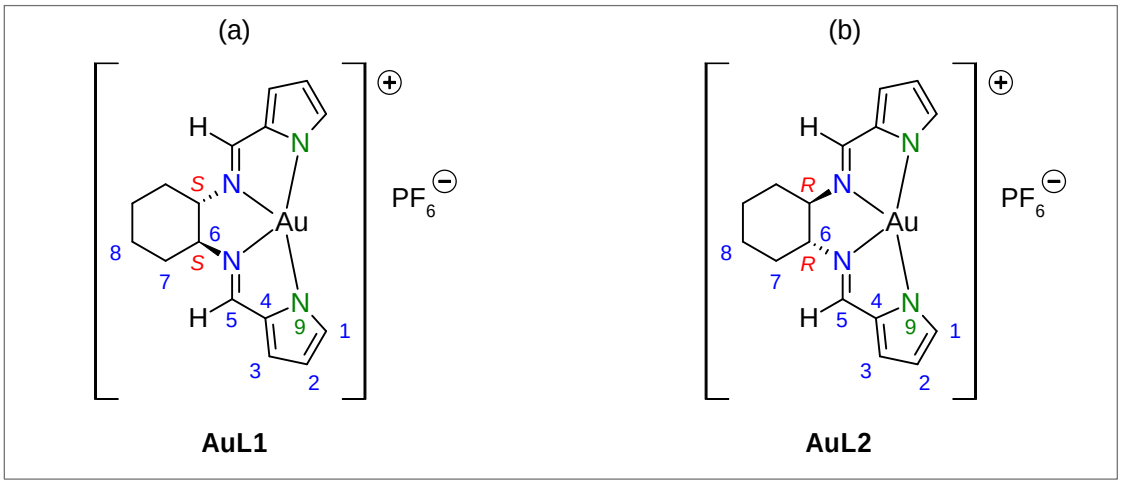

Scheme 2. Structures of (a) [Au((1S,2S)**L1**)PF_6 (**AuL1**) and (b) [Au((1R,2R)**L2**)]PF_6 (**AuL2**). The atom numbering scheme is indicated. The enantiomeric complexes were analysed by ^{1}H NMR, ^{13}C NMR, ^{19}F NMR and ^{32}P NMR, UV-visible spectroscopy, mass spectroscopy, and FT-IR spectroscopy as well as single crystal X-ray diffraction.

^{1}H NMR (400 MHz, DMSO-d_6) δ 8.38 (s, 1H, H-5), 7.80 (d, J = 2.0 Hz, 1H, H-1), 7.07 (d, J = 4.2 Hz, 1H, H-3), 6.47 (dd, J = 4.2, 2.1 Hz, 1H, H-2), 4.30 (d, J = 9.0 Hz, 1H, H-6), 2.61 (d, J = 12.2 Hz, 1H, H-7), 1.77 (d, J = 9.1 Hz, 1H, H-7), 1.62 (d, J = 10.2 Hz, 1H, H-8), 1.34 (q, J = 11.4, 10.4 Hz, 1H, H-8). ^{13}C NMR (101 MHz, DMSO-d6) δ 157.70 (C-5), 142.16 (C-1), 138.80 (C-4), 123.98 (C-3), 111.72 (C-2), 75.68 (C-6), 27.95 (C-7), 22.94 (C-8). ^{31}P NMR (162 MHz, DMSO-d_6) δ −127.11 – −158.79 (m). ^{19}F NMR (376 MHz, DMSO-d_6) δ −70.16 (d, J = 711.2 Hz). **AuL1** IR (cm^{-1}): 2948m br ν(CH, imine), 1563s br ν(C=N), 822s ν(PF_6). **AuL2** IR (cm^{-1}): 2945m br ν(CH, imine), 1564s br ν(C=N), 826s ν(PF_6). ESI-MS: m/z+ = 463.1276 (**AuL1**) and 463.1284 (**AuL2**); M+ (463.1197). UV-vis (MeCN) [λ_{max}, nm (ε, mol^{-1} dm^3 cm^{-1})]: 288 (1.15×10^4); 382 (0.47×10^4).

1.3 Fluorescence Spectroscopy

Fluorescence measurements were performed on a Cary Eclipse fluorescence spectrophotometer (Varian, Australia) equipped with a 1.0 cm quartz cell and a circulating thermostat bath. The HSA concentration was kept at 5.0×10^{-6} mol dm^{-3} and the excitation and emission slit widths were fixed at 5 nm. The concentrations of **AuL1** and **AuL2** ranged from 0 to 98×10^{-6} mol dm^{-3}. Both gold(III) chelates were made up in MeCN and the final MeCN concentration was under 0.1% (V/V) to prevent denaturation of HSA. HSA was excited at 295 nm (excitation of Trp-214), and the emission spectra were recorded from 310 to 400 nm. Spectral titrations were carried out at three temperatures (288, 298 and 310K) in triplicate.

Correction of fluorescence data. An inner filter effect (IFE) correction was applied to all fluorescence data using eq. S1.[10]

$$F_{corrected} = F_{observed} * 10^{Aex*dex+Aem*dem} \quad \text{S1}$$

Where A_{ex} and A_{em} are the absorbance readings at the excitation and emission wavelengths and *d* is the path length of the cuvette. The correction is required when the added ligand (metal chelate) absorbs significantly at the excitation and emission wavelengths of the fluorophore being analysed.

Further corrections to the concentration of **AuL1** and **AuL2** were not required as the concentration of both Au(III) chelates >> than [HSA].[11]

$$[Ligand]_{free} = [Ligand]_{added} \quad \text{S2}$$

Fluorescent probe displacement assay. Warfarin and dansylglycine were used as specific site marker fluorescent probes for Sudlow's sites I and II, respectively. Steady-state fluorescence spectra were recorded as described above at 298 K using 10 nm excitation and emission bandwidths for warfarin, while 5 nm excitation and 10 nm emission band widths were employed for dansylglycine. The fluorophores warfarin and dansylglycine were equilibrated (bound) to HSA (50 mM KH_2PO_4 buffer, pH 7.50) and were excited at 320 nm and 340 nm, respectively. The emission spectrum was measured in the range 350 – 500 nm for warfarin and 400 – 650 nm for dansylglycine. The HSA and fluorescence probe concentrations were both used at 5.0 μM. Titrations were performed by increasing the concentrations of **AuL1** and **AuL2** in the protein-probe solution from 0 to 98 μM for warfarin and 0 to 78 μM for dansylglycine.

1.4 Circular dichroism (CD) spectroscopy

Far UV CD spectra of solutions of HSA (5.0×10^{-9} mol dm^{-3}) in the absence and presence of increasing concentrations (0 – 6 μM) of **AuL1** and **AuL2** were recorded with a JASCO J-1500 CD spectrometer equipped with a Peltier temperature controller (25 °C). A scan speed of 100 nm min^{-1} was employed for spectral acquisition with a 0.5 nm data pitch and a response time of 2 s. Each spectrum was the average of three scans. Spectra were recorded over a wavelength range of 190–260 nm (0.4 cm pathlength quartz cuvette). All spectra were processed with JASCO Spectral Manager™.

Near UV-vis CD spectra (250–500 nm, 1.0-cm pathlength quartz cuvette, 25 °C) were recorded similarly to detect induced CD (ICD) signals of the achiral ligands and metal chelates upon their uptake by HSA. Typically, HSA (15.0×10^{-6} M) was incubated with a saturating dose (15×10^{-6} M) of either **AuL1** or **AuL2** for at least 60 min. A scan speed of 200 nm min^{-1} was used with a 0.5-nm data pitch (response time, 2 s); each spectrum was the average of three scans.

1.5 *In vitro* cell screening

The method given here is a restatement (for completeness) of that published and used by the DTP,[12] to which **AuL1** and **AuL2** were submitted for in vitro cytotoxicity screening. The human tumour cell lines of the NCI-60 cancer screening panel are grown in RPMI 1640 medium containing 5% foetal bovine serum and 2 mM of the amino acid L-glutamine. For most screening experiments, cells are inoculated into 96-well microtiter plates in 100 μL of solution with plating densities between 5×10^3 and 4×10^4 cells per well, depending on the doubling time of a particular cell line. After cell inoculation, the 96- well plates are incubated at 37 °C, with an atmospheric composition of 5% CO_2 and 95% air at 100% relative humidity for 24 hours prior to addition of experimental drugs. After 24 hours, two plates of each cell line are fixed *in situ* with tricarboxylic acid (TCA), to represent a measurement of the cell population for each cell line at the time of drug addition (Tz). Experimental drugs are dissolved in DMSO at a concentration 400× that of the maximum desired test concentration and stored frozen prior to use. As required, an aliquot of frozen drug concentrate is thawed and diluted to twice the desired maximum test concentration with appropriate medium, containing 50 μg ml^{-1} of gentamicin (an aminoglycoside

antibiotic). Four, 10-fold serial dilutions are carried out to provide a total of five drug concentrations as well as a control. Aliquots of 100 µl of these different drug dilutions are added to the appropriate wells already containing 100 µl of medium, resulting in the required final drug concentrations.

Following drug addition, the plates are incubated for an additional 48 hours at 37 °C, with an atmosphere consisting of: 5% CO_2, 95% air, and 100% relative humidity. For adherent cells, the assay is terminated by the addition of cold TCA. Cells are fixed *in situ* by the gentle addition of 50 µl of cold 50% (w/v) TCA (final concentration, of 10% TCA) and incubated for 1 hour at 4 °C. The supernatant liquid is discarded, and the plates are washed repeatedly with water and air dried. Sulforhodamine B (SRB) solution (100 µl) with a concentration of 0.4% (w/v) in 1% acetic acid is added to each well, and plates are incubated for 10 minutes at room temperature. After staining, unbound dye is removed by washing repeatedly with 1% acetic acid solution and the plates are again air dried. Bound stain is subsequently solubilised with 10 mM tris(hydroxymethyl)aminomethane base, and the absorbance is read on an automated plate reader at a wavelength of 515 nm, which corresponds to λ_{max} of the dye used. This is a method of transcriptional and translational (MTT) assay. For suspension cells, the methodology is the same as above with the exception that the assay is terminated by fixing settled cells at the bottom of the wells by adding 50 µl of 80% TCA (final concentration, 16% TCA).

Using the seven absorbance measurements: time zero, (Tz), control growth, (C), and test growth in the presence of the gold(III) chelate at the five concentration levels (Ti), the percentage growth is calculated at each of the drug concentrations. Percentage growth inhibition is calculated as:

$$\left(\frac{T_i - T_z}{C - T_2}\right) x\ 100\% \qquad \text{S3}$$

$$\left(\frac{T_i - T_z}{T_2}\right) x\ 100\% \qquad \text{S4}$$

Eq. S3 is applicable for concentrations for which Ti ≥ Tz, while eq. S4 is applicable for drug concentrations at which Ti < Tz. Three dose response parameters are then calculated for each experimental compound from the data collected. Firstly, GI_{50} is calculated from:

$$\left(\frac{T_i - T_z}{C - T_2}\right) x\ 100\% = 50 \qquad \text{S5}$$

Secondly, (TGI or IC_{50}) is calculated from:

$$Ti = Tz \qquad \text{S6}$$

Thirdly LC_{50} is calculated from:

$$\left(\frac{T_i - T_z}{T_2}\right) x\ 100\% = -50 \qquad \text{S7}$$

1.6 GSH reacting with AuL1

AuL1 (100 µM) was reacted with GSH at either 100 µM or 1 mM in 50 mM KH_2PO_4 buffer. The reaction was monitored using UV-vis spectroscopy over 3 h in 15 min time intervals from 250 – 600 nm.

1.7 The reaction of AuL1 with ctDNA

Stock solution of calf thymus DNA (ctDNA) was prepared by dissolving the sodium salt (Sigma-Aldrich) in KH_2PO_4 buffer (pH 7.5, 50 mM) and slowly agitating it overnight at 70 rpm. The concentration of the solution was determined spectrophotometrically (ε=13 200 M^{-1} cm^{-1} at 260 nm).[19] In brief gold(III) chelates were prepared in KH_2PO_4 buffer and DMSO and diluted to a concentration of ± 50 µM. Increasing concentrations of ctDNA was added to the gold(III) chelates that were incubated at 37 °C and the absorbance spectra was recorded from 250 – 500 nm using a Analytik Jena Specord210 Plus double-beam instrument fitted with an external water circulating thermostatic bath and thermostatted cell holders. Measurements were carried out in triplicates using 1.0 cm quartz cuvettes.

2. Figures and Tables

2.1 General Characterisation Data

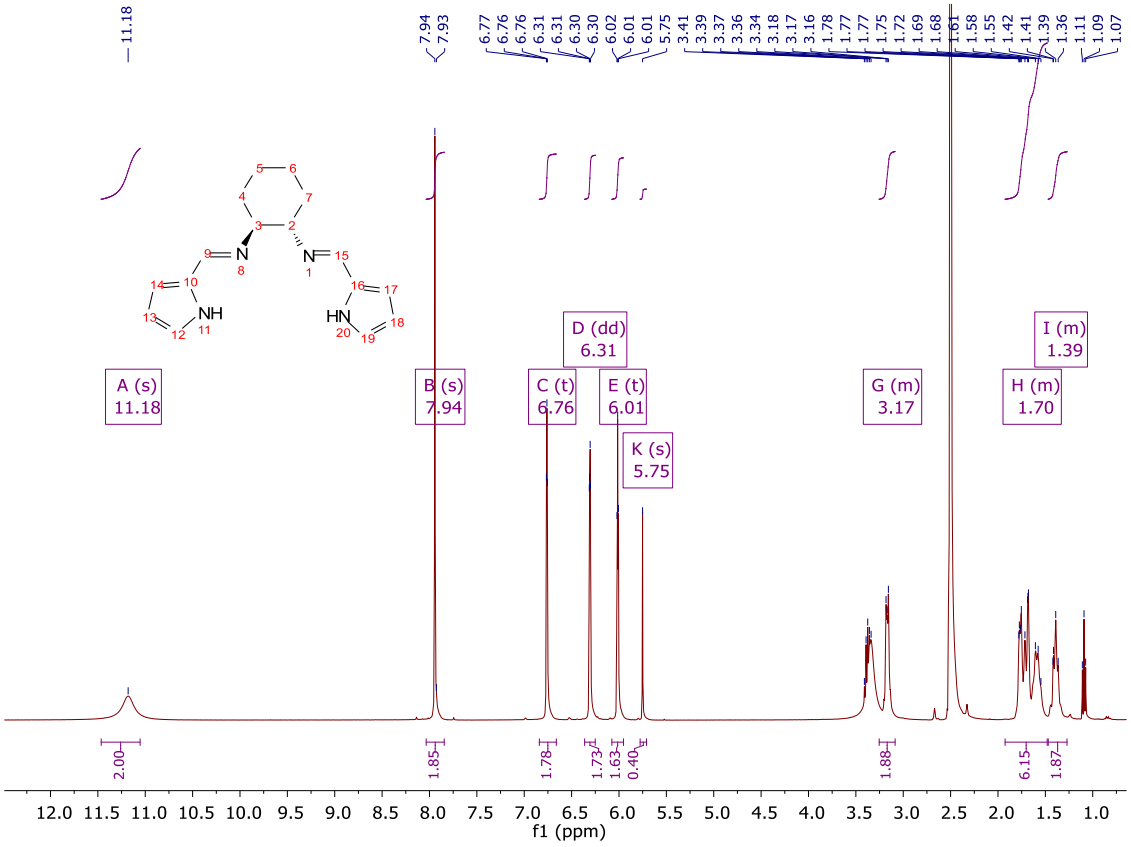

Fig. S1 ^{1}H NMR of **H_2L1** in DMSO–d6.

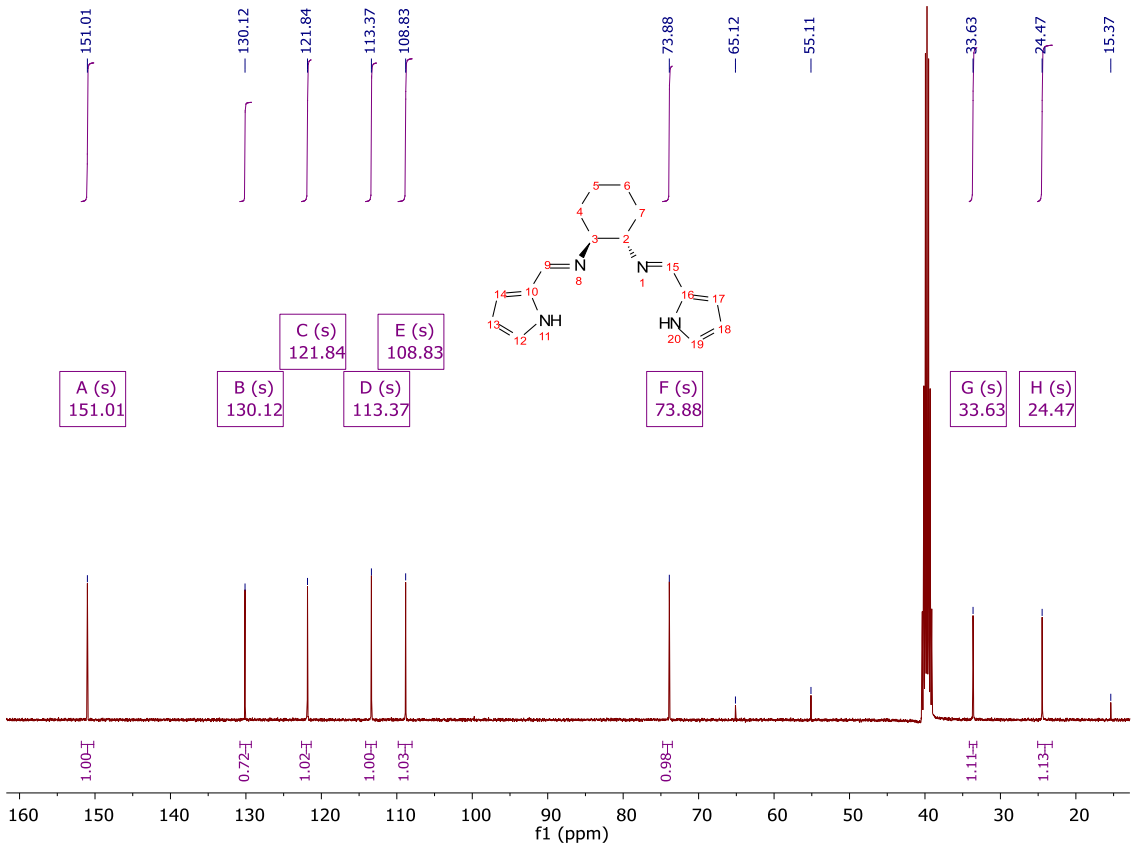

Fig. S2 ^{13}C NMR of **H_2L1** in DMSO–d6.

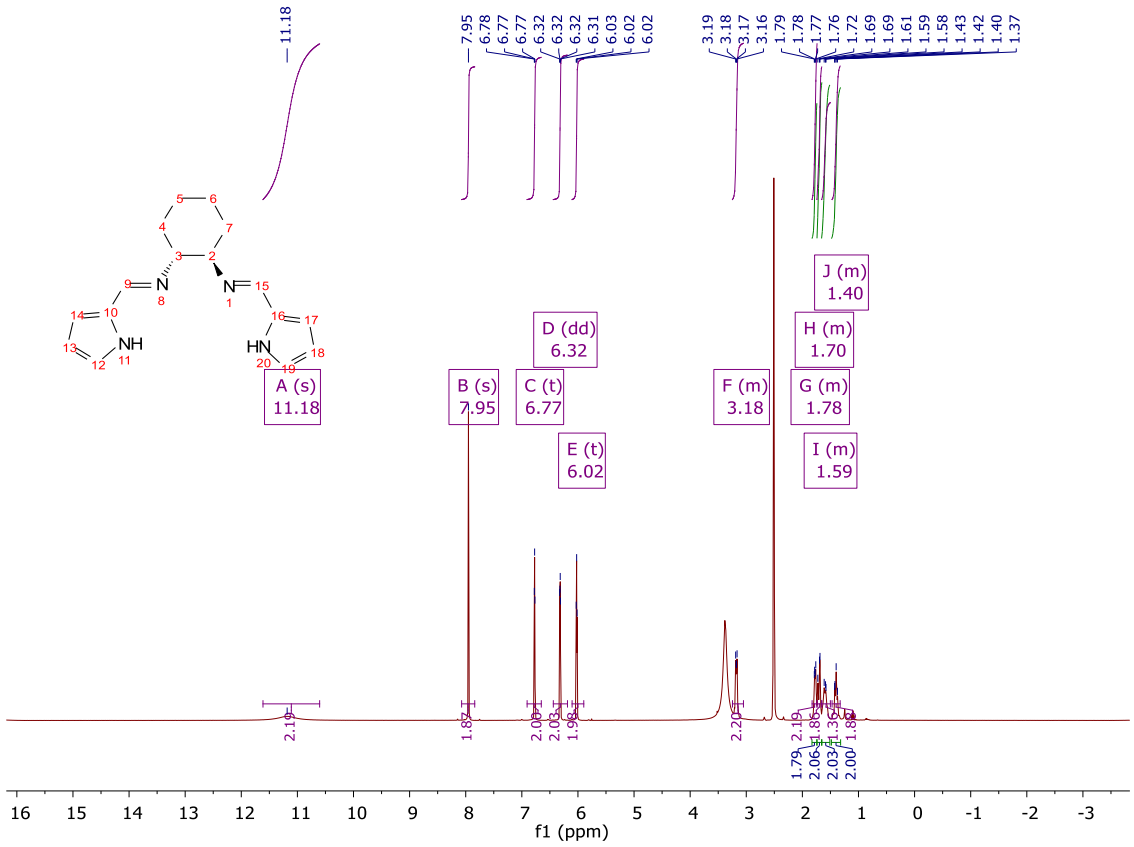

Fig. S3 ^{1}H NMR of **H_2L2** in DMSO–d6.

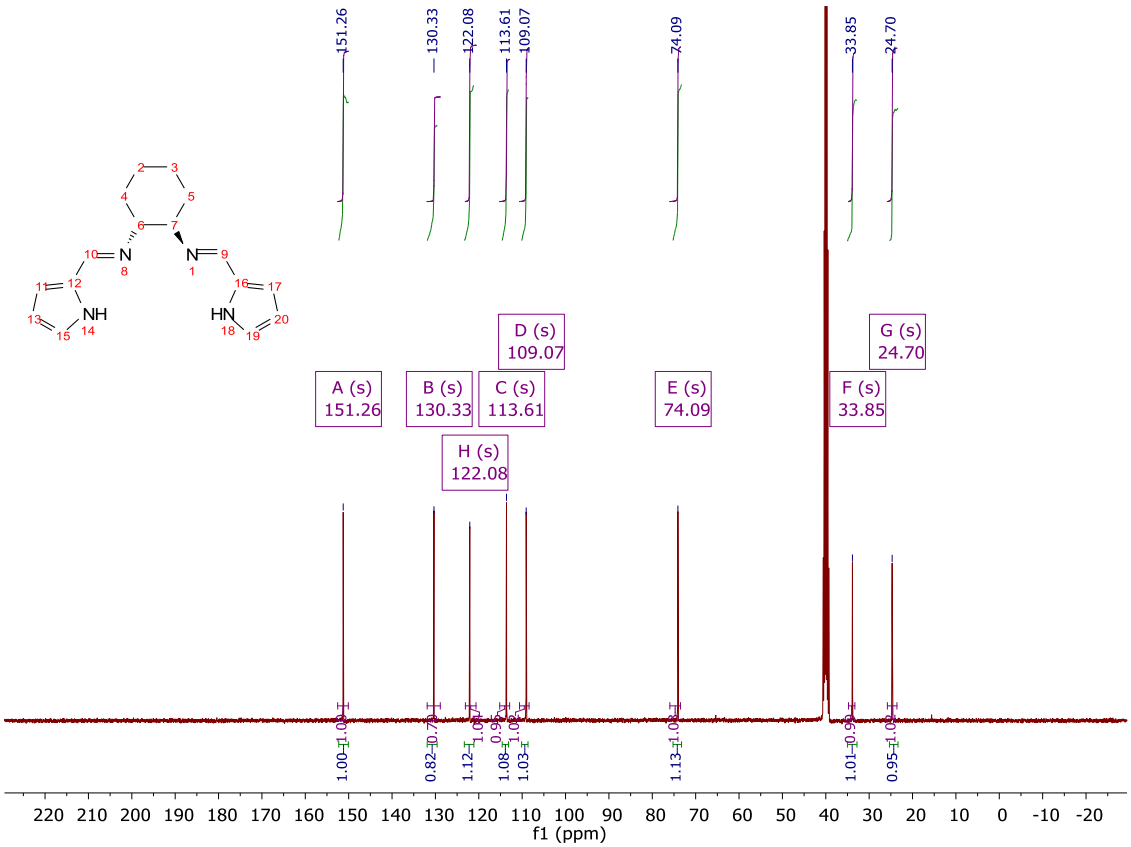

Fig. S4 ^{13}C NMR of **H_2L2** in DMSO–d6.

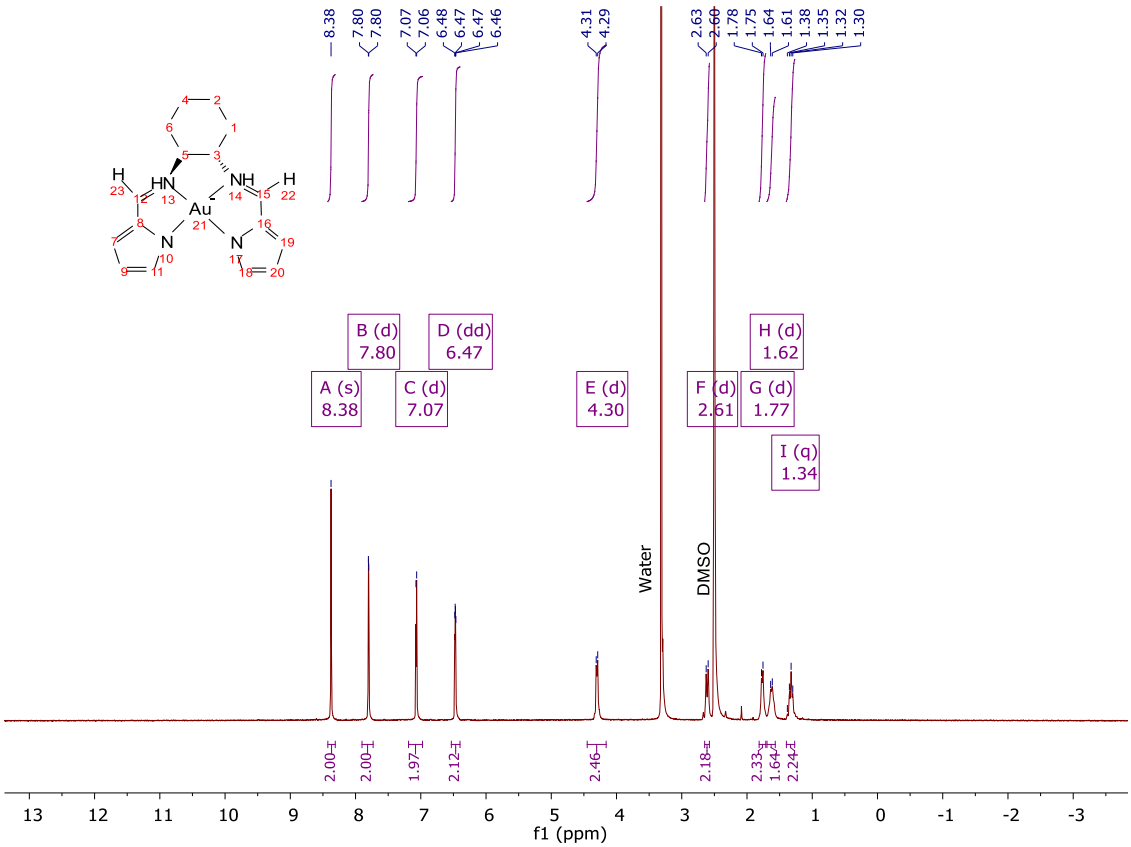

Fig. S5 ^{1}H NMR of **AuL1** in DMSO–d6.

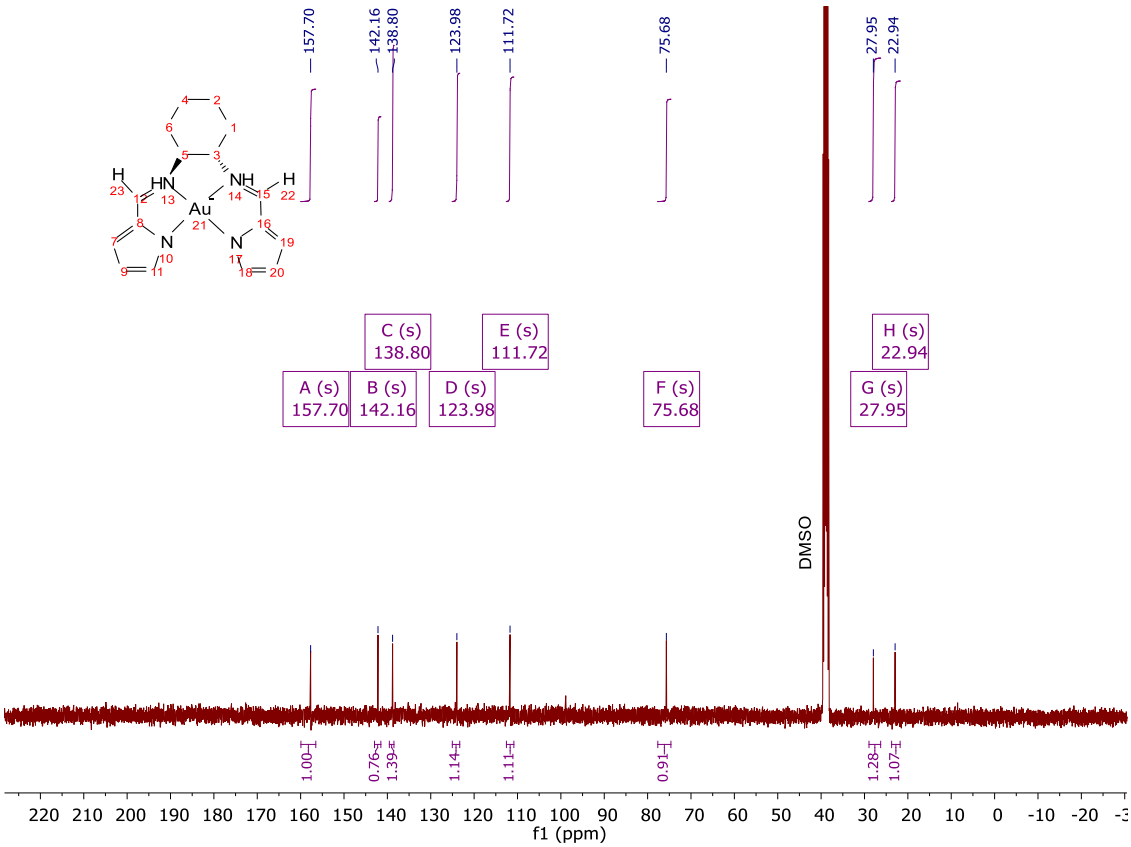

Fig. S6 ^{13}C NMR of **AuL1** in DMSO–d6.

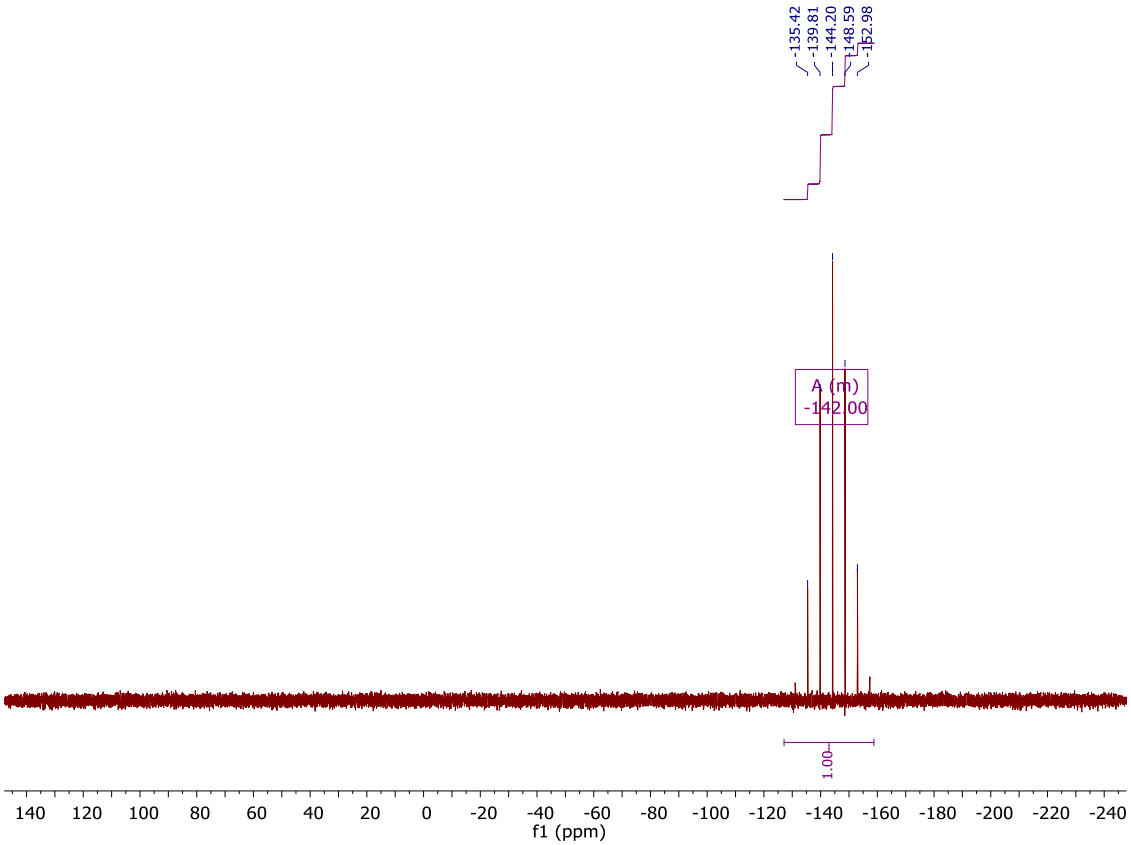

Fig. S7 ^{31}P NMR of **AuL1** in DMSO–d6

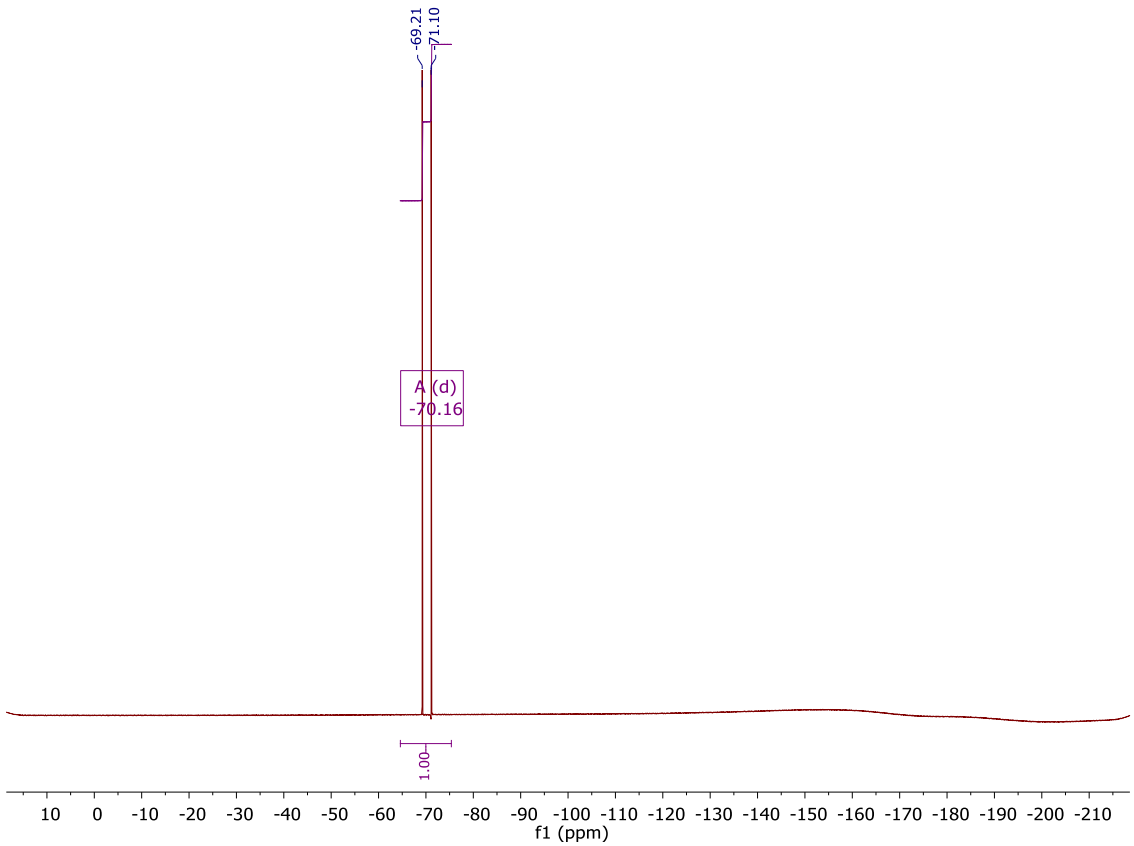

Fig. S8 ^{19}F NMR of **AuL1** in DMSO–d6

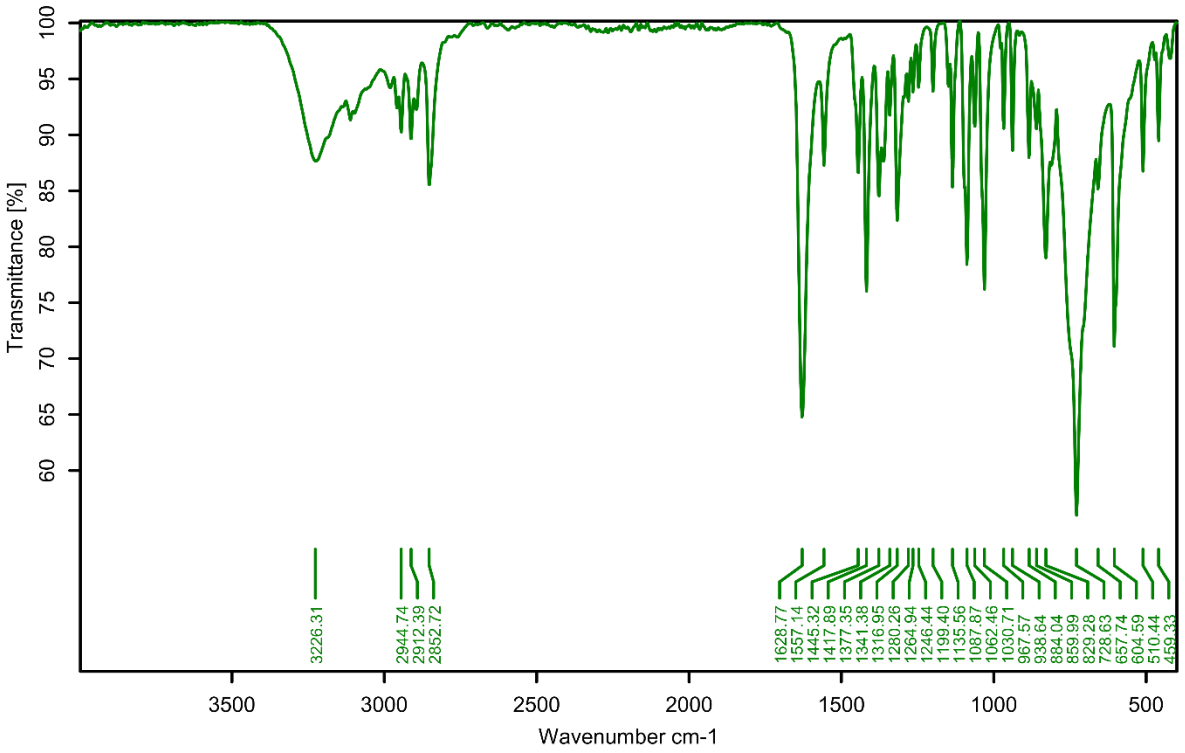

Fig. S9 FT-IR spectrum of **H_2L1** recorded as a crushed powder sample at 298 K.

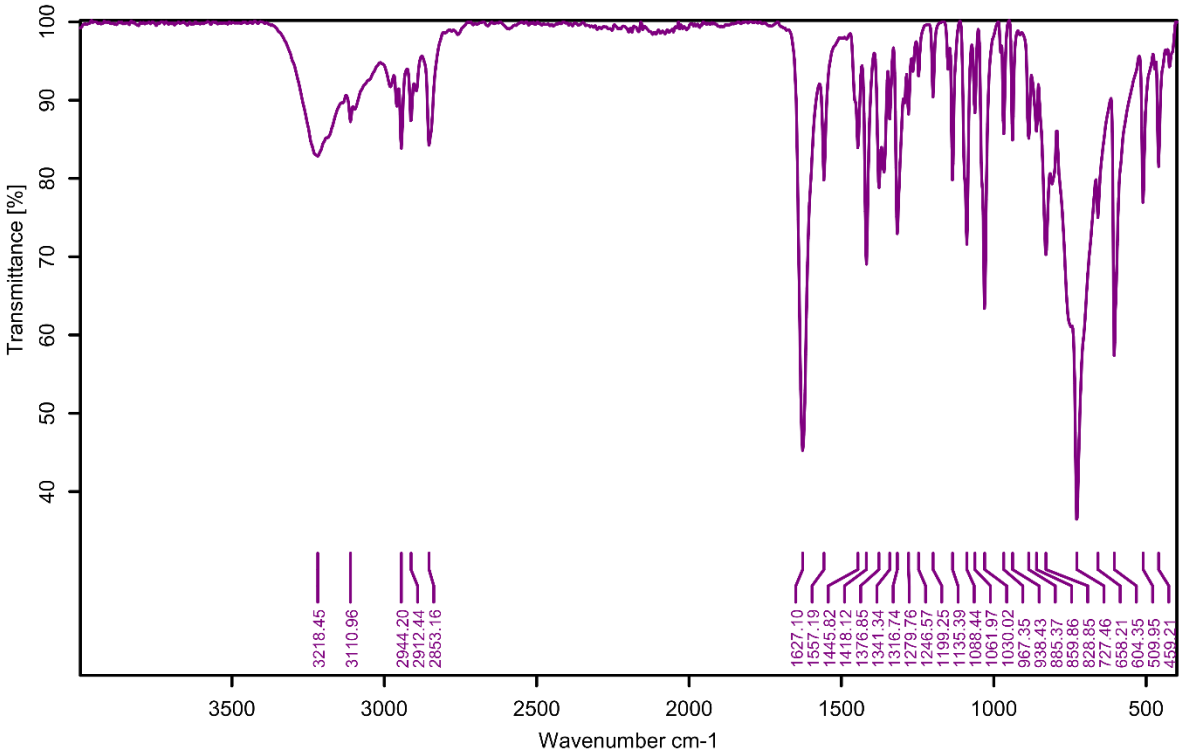

Fig. S10 FT-IR spectrum of **H_2L2** recorded as a crushed powder sample at 298 K.

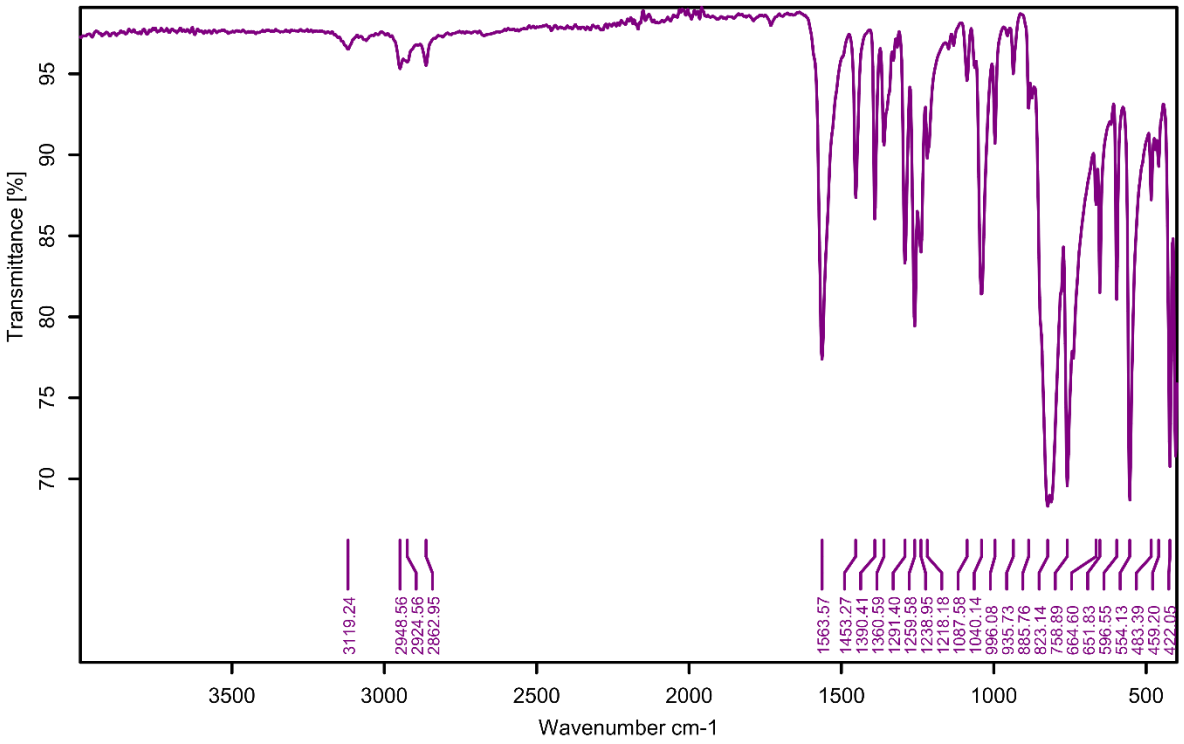

Fig. S11 FT-IR spectrum of **AuL1** recorded as a crushed powder sample at 298 K.

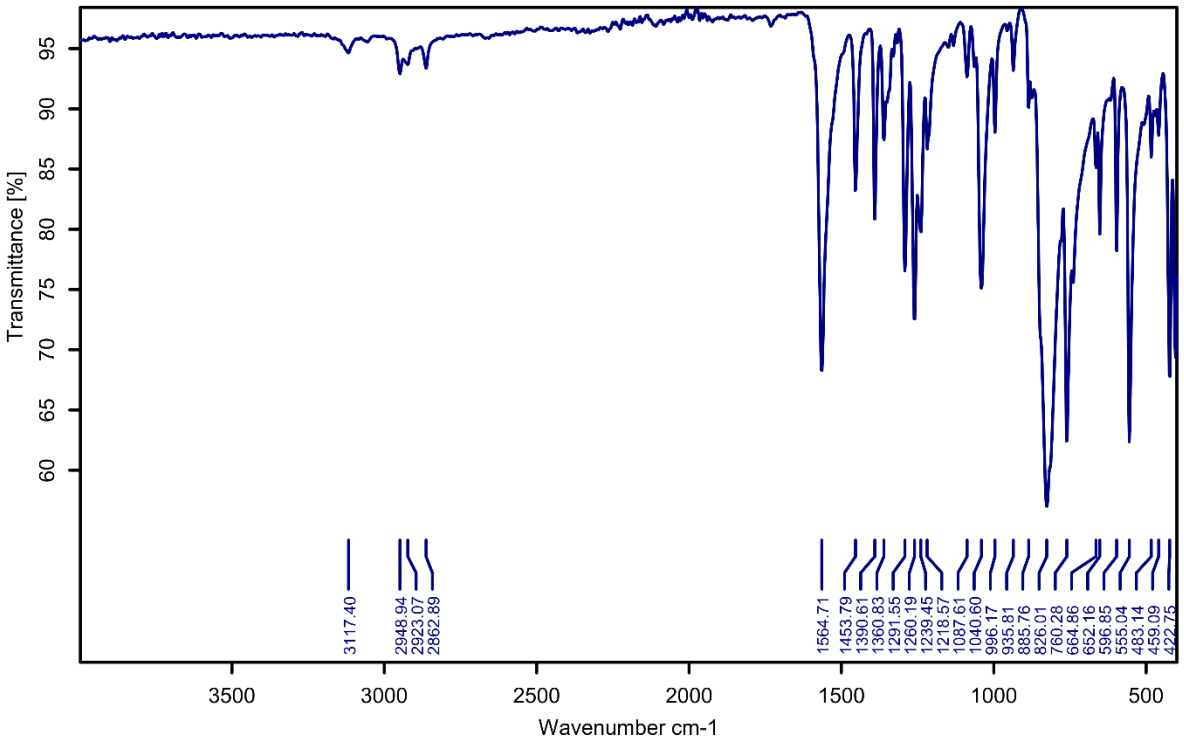

Fig. S12 FT-IR spectrum of **AuL2** recorded as a crushed powder sample at 298 K.

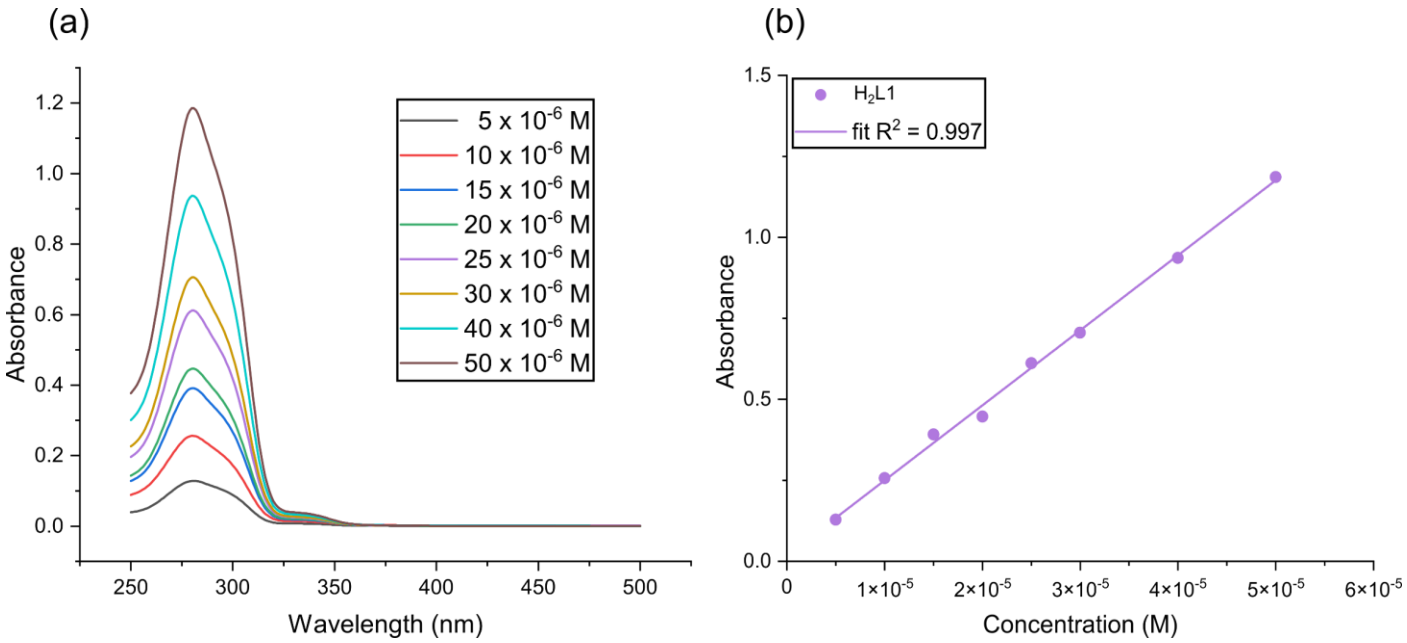

Fig. S13 UV-visible spectrum of **H_2L1** recorded in acetonitrile at 298 K as a function of concentration. The molar absorptivity of the band maximum is reported in the characterisation data and was determined from (b) the slope of a Beer-Lambert law plot at the relevant band maximum.

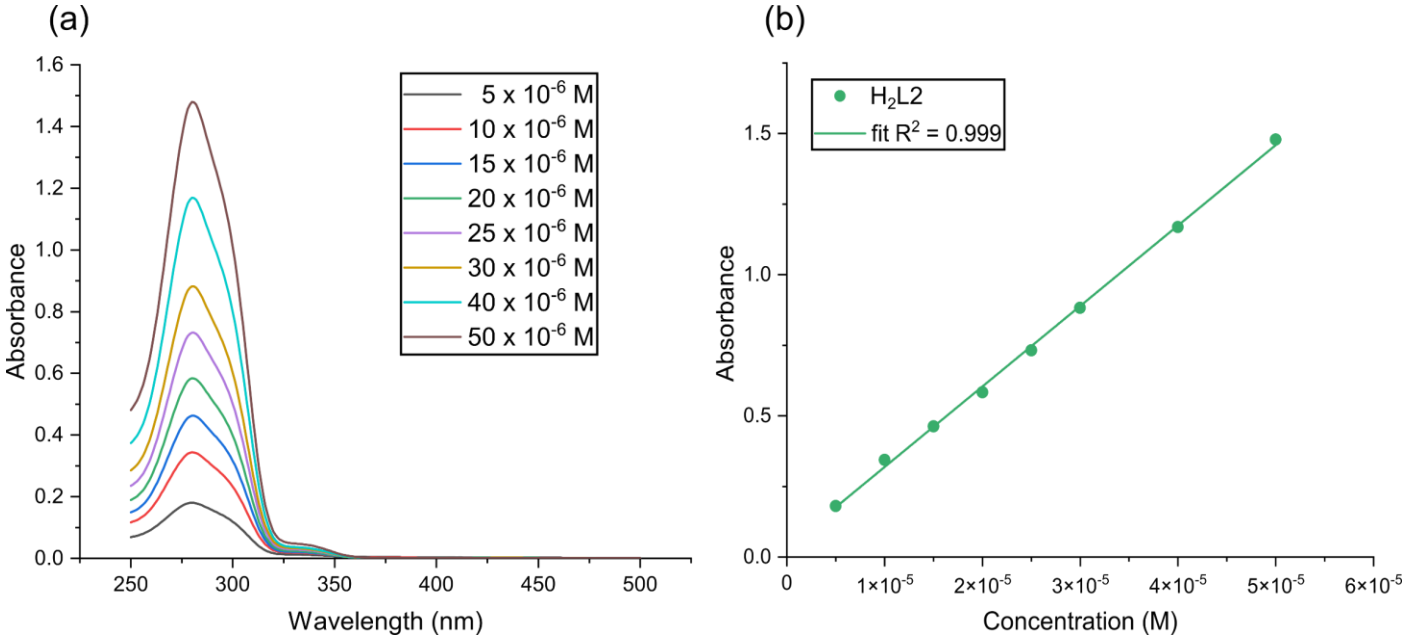

Fig. S14 UV-visible spectrum of **H_2L2** recorded in acetonitrile at 298 K as a function of concentration. The molar absorptivity of the band maximum is reported in the characterisation data and was determined from (b) the slope of a Beer-Lambert law plot at the relevant band maximum.

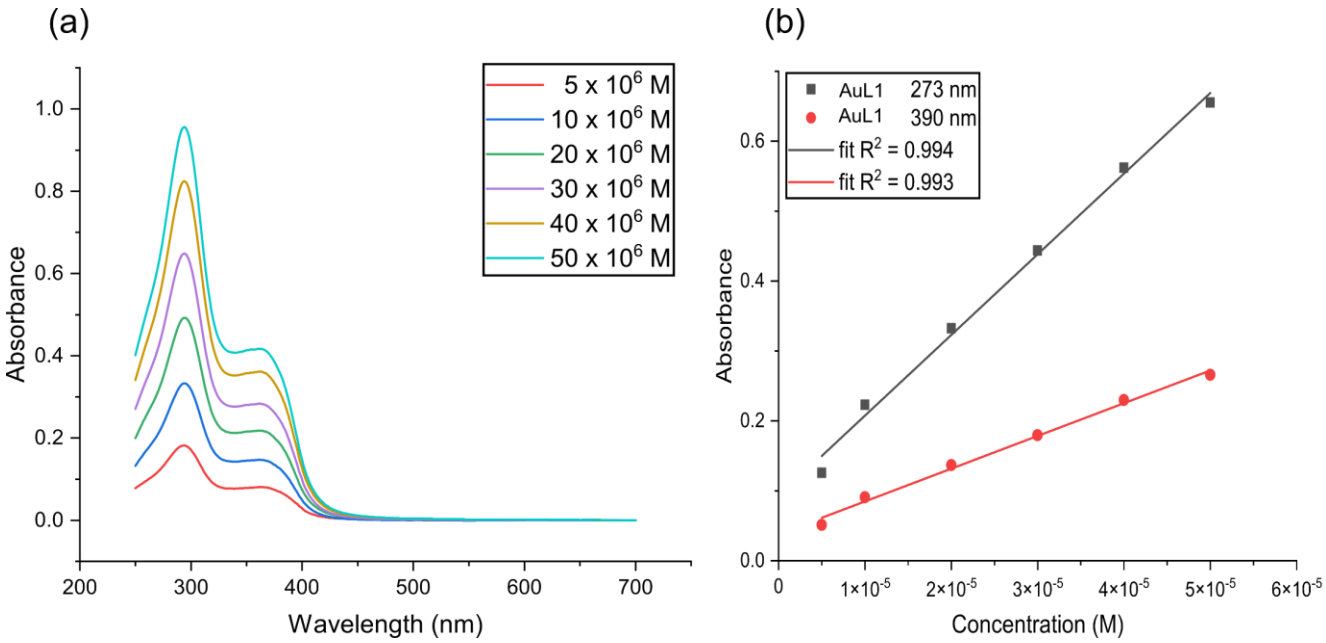

Fig. S15 UV-visible spectrum of **AuL1** recorded in acetonitrile at 298 K as a function of concentration. The molar absorptivities of key band maximum are reported in the characterisation and were determined from (b) the slopes of Beer-Lambert law plots at the relevant band maxima.

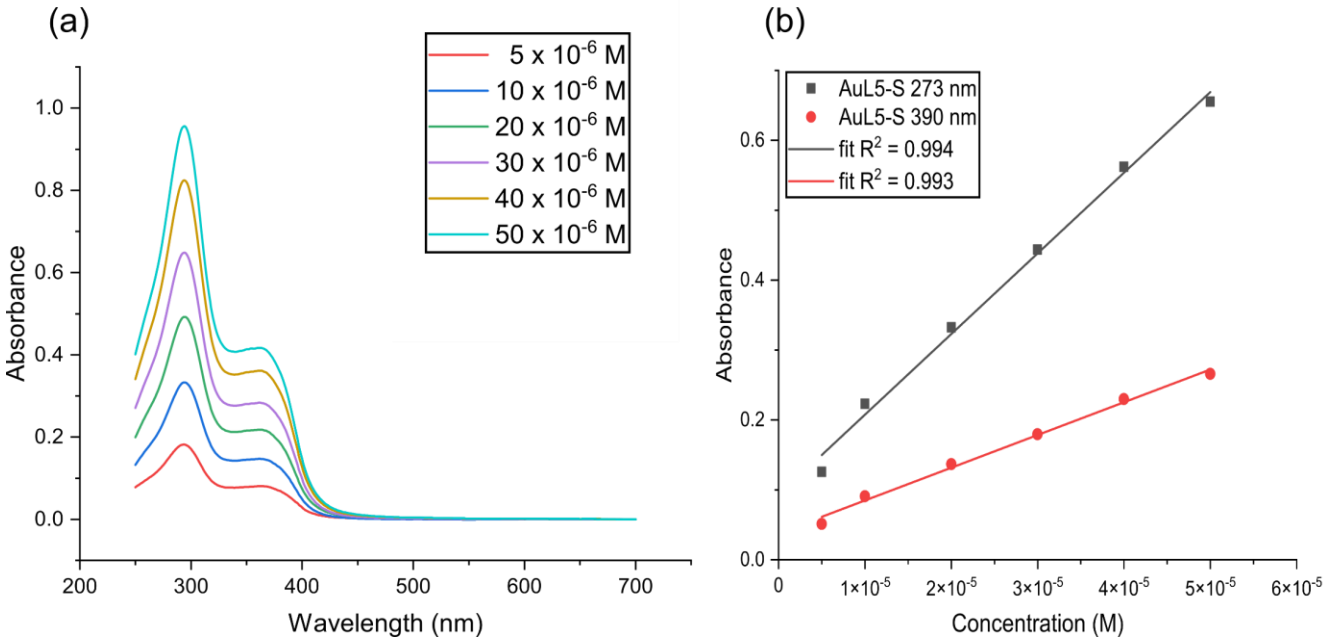

Fig. S16 UV-visible spectrum of **AuL2** recorded in acetonitrile at 298 K as a function of concentration. The molar absorptivities of key band maxima are reported in the characterisation data and were determined from (b) the slopes of Beer-Lambert law plots at the relevant band maxima.

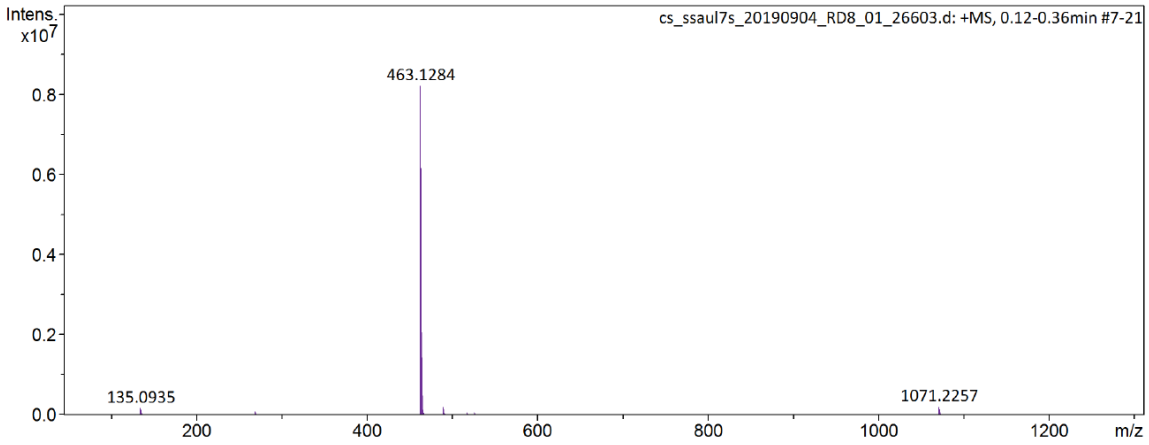

Fig. S17 ESI-MS spectrum of **AuL1**. The solid sample was dissolved in methanol with 0.1% formic acid (V/V) and the spectrum was recorded in positive ESI mode.

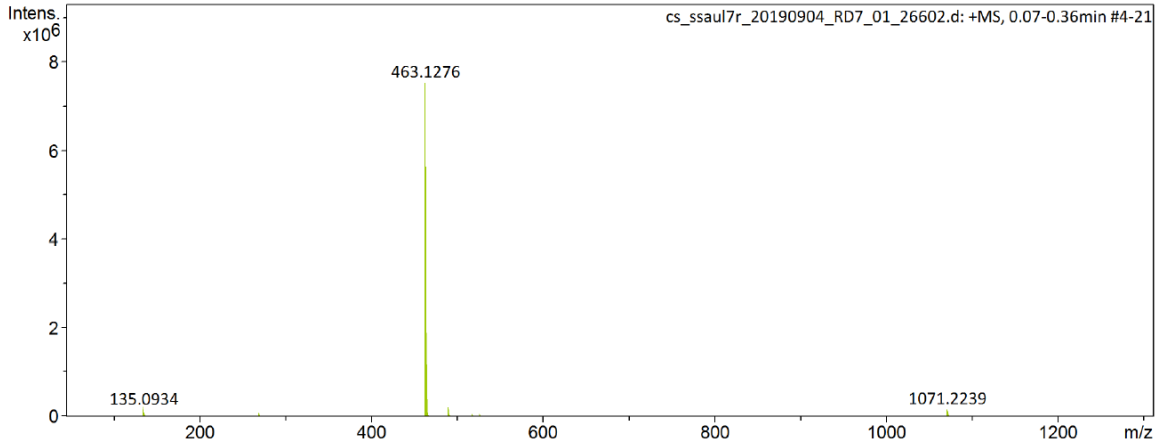

Fig. S18 ESI-MS spectrum of **AuL2**. The solid sample was dissolved in methanol with 0.1% formic acid (V/V) and the spectrum was recorded in positive ESI mode.

2.2 Fluorescence spectroscopy

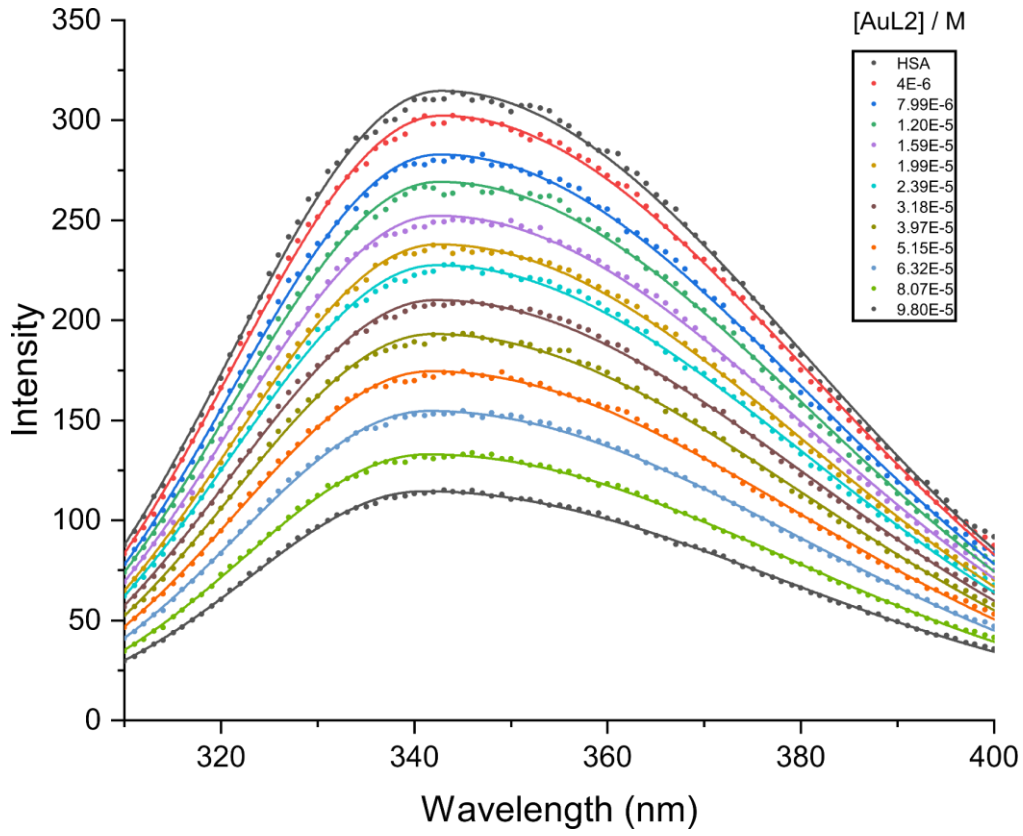

Fig. S19 Fluorescence emission spectra of HSA (5.0 µM) recorded as a function of increasing concentration of **AuL2** at 298 K. The emission spectra confirm that **AuL2** quenches the intrinsic HSA (i.e., Trp-214) fluorescence upon binding.

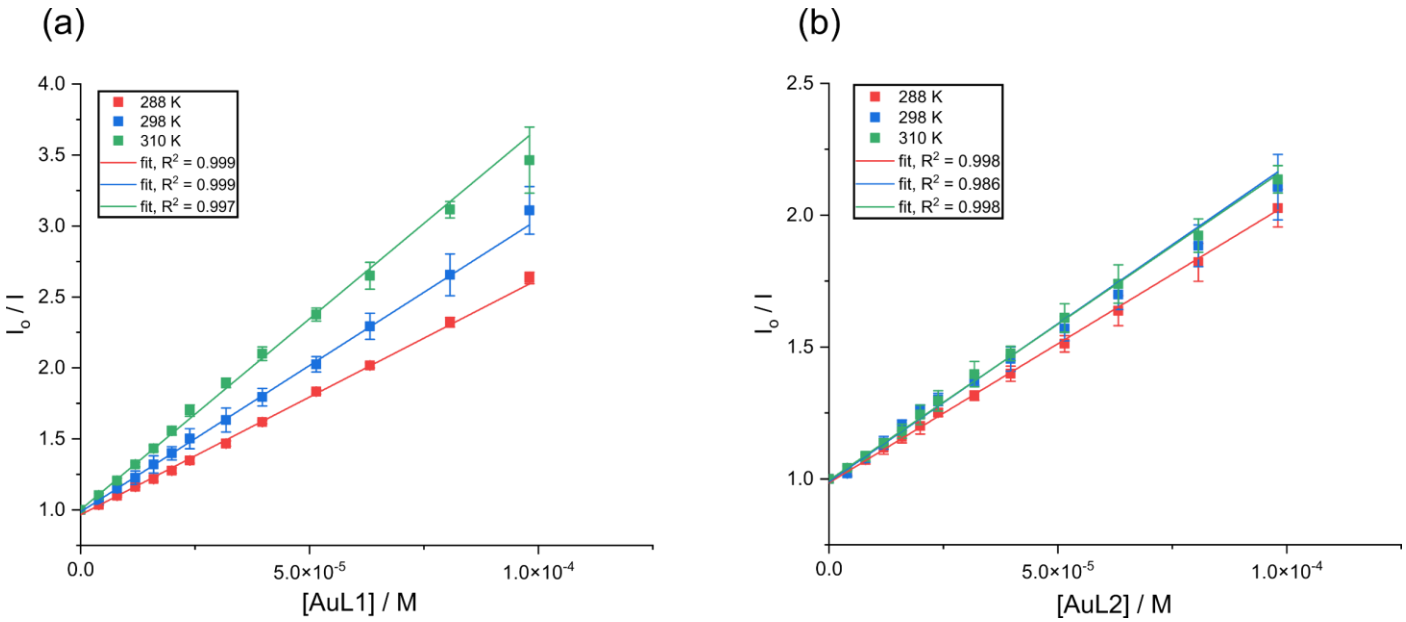

Fig. S20 Stern–Volmer plots of fluorescence quenching: **(a) AuL1**···HSA complex and **(b) AuL2**···HSA complex. Data for both gold(III) chelates were recorded at three different temperatures (■ 288 K, ■ 298 K, and ■ 310 K). The relevant concentrations for the titrations were: [HSA] = 5.0 µM, and the gold(III) chelates were 0 – 98 µM in KH_2PO_4 buffer (pH 7.50 in 50 mM). Error bars indicate the standard deviation of three independent experiments.

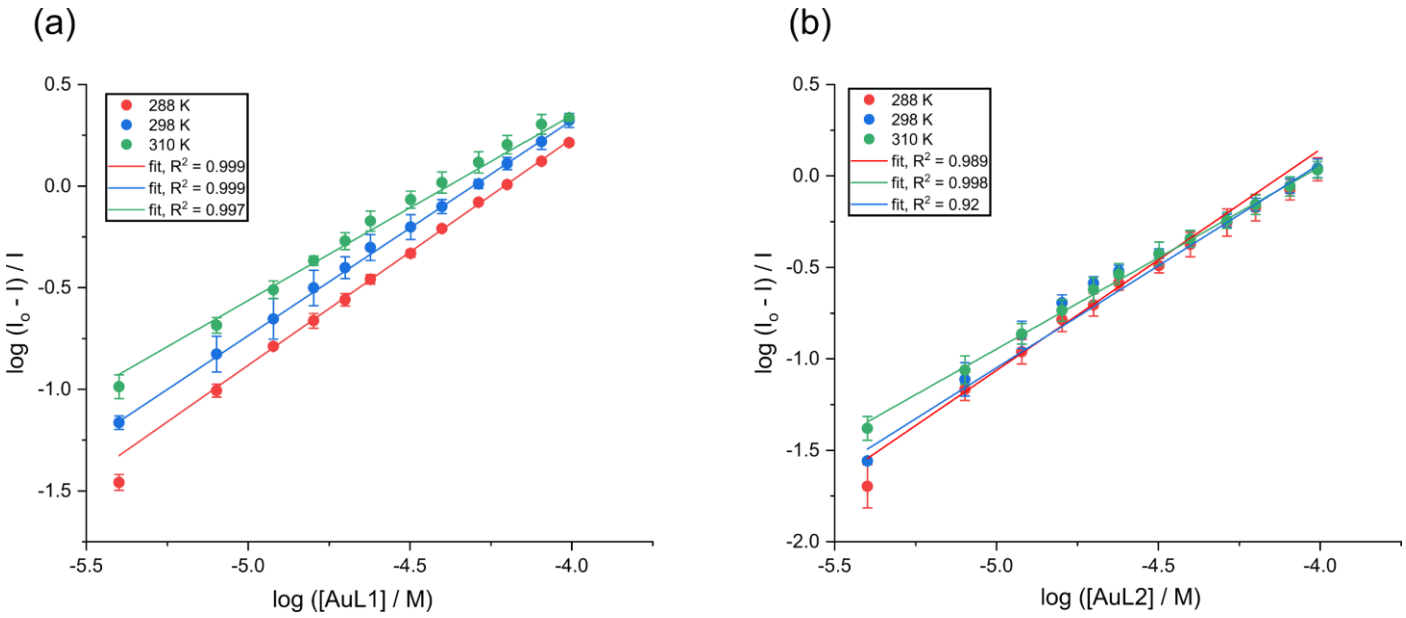

Fig. S21 Plots of log((I₀-I)/I) versus log([Q]) for the interaction of HSA with the two enantiomeric gold(III) chelates (i.e., quenchers, Q): (a) **AuL1**···HSA complex, (b) **AuL2**···HSA complex. The affinity constants are determined from the intercepts of the graphs and the stoichiometry from the slopes. Data for the gold(III) chelate···HSA systems were recorded at three different temperatures (, ● 288 K, , ● 298 K, and, ● 310 K) The relevant concentrations for the titrations were: [HSA] = 5.0 µM, and the gold(III) chelates ranged from 0 – 9.8 × 10^{-5} M at pH 7.50 in 50 mM KH_2PO_4 buffer.

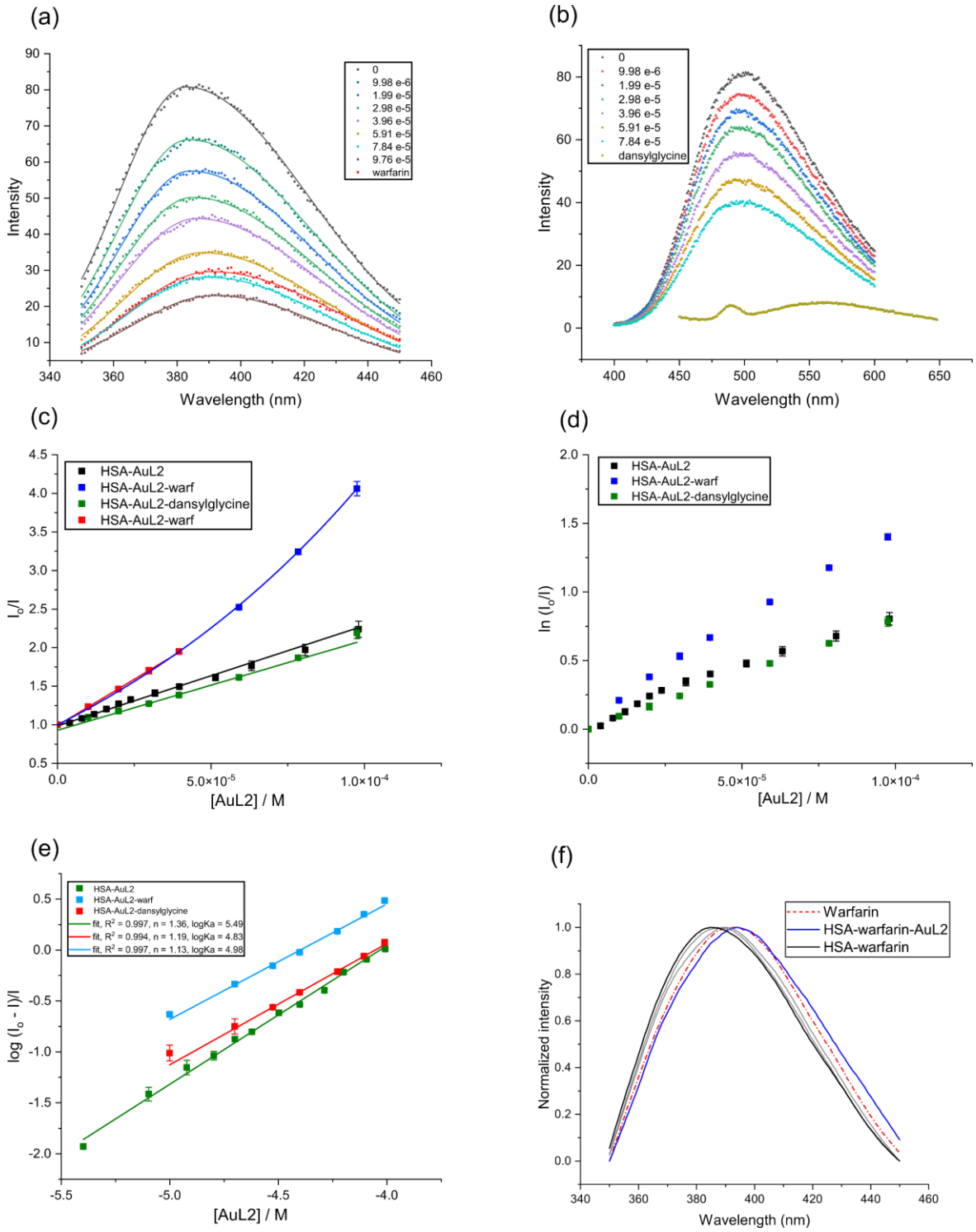

Fig. S22 Binding site determination for the reaction of **AuL2** with HSA (5.0 μM protein, 50 mM KH_2PO_4, pH 7.50, 298 K). **(a)** Emission spectra of HSA···warfarin (5.0 μM warfarin λ^{ex} = 320 nm) recorded as a function of the concentration of AuL4-R at 298 K. The spectra are fitted by single Gaussian functions to locate the emission maxima. Correlation coefficients, R^2, ranged from 0.990 to 0.999. **(b)** Emission spectra of HSA···dansylglycine (5.0 μM dansylglycine λ^{ex} = 340 nm) recorded as a function of the concentration of AuL4-R at 298 K. The spectra are fitted by single Gaussian functions to locate the emission maxima. Correlation coefficients, R^2, ranged from 0.990 to 0.999. **(c)** Stern–Volmer (SV) plot for native HSA, HSA···Warfarin, and HSA···dansylglycine as a function of the concentration of **AuL2** at 298 K. The plots are linear with an intercept of 1.0 when static quenching is operative (i.e., the quencher binds to the target protein and fluorophore(s)). The excitation and emission wavelengths for the fluorophore probes were: (i) Trp-214 (native HSA), λ^{ex} = 295 nm, λ^{em} = 340 nm; (ii) Warfarin (HSA-Warf), λ^{ex} = 320 nm, λ^{em} = 382 nm, and (iii)

dansylglycine, λ^{ex} = 340 nm, λ^{em} = 500 nm. **(d)** Sphere of action model plot, $ln\left(\frac{I_0}{I}\right) = K_{SV}^{app}[Q]$, for the system. A linear plot with a zero intercept indicates static quenching by AuL4-R bound in some way to the fluorophore/macromolecule. Negative deviation from linearity signals a switch from static to dynamic quenching. **(e)** Double-log plot (eq. 10) of the fluorescence quenching data, $log\left(\frac{I_0-I}{I}\right) = logK + nlog[Q]$, to enable measurement of logKa and the reaction stoichiometry (n). **(f)** Normalized fluorescence emission spectrum of HSA···warfarin (5.0 μM warfarin λ^{ex} = 320 nm) recorded as a function of the concentration of **AuL2** at 298 K to show the displacement of warfarin from HSA. Error bars indicate the standard deviation of three independent experiments.

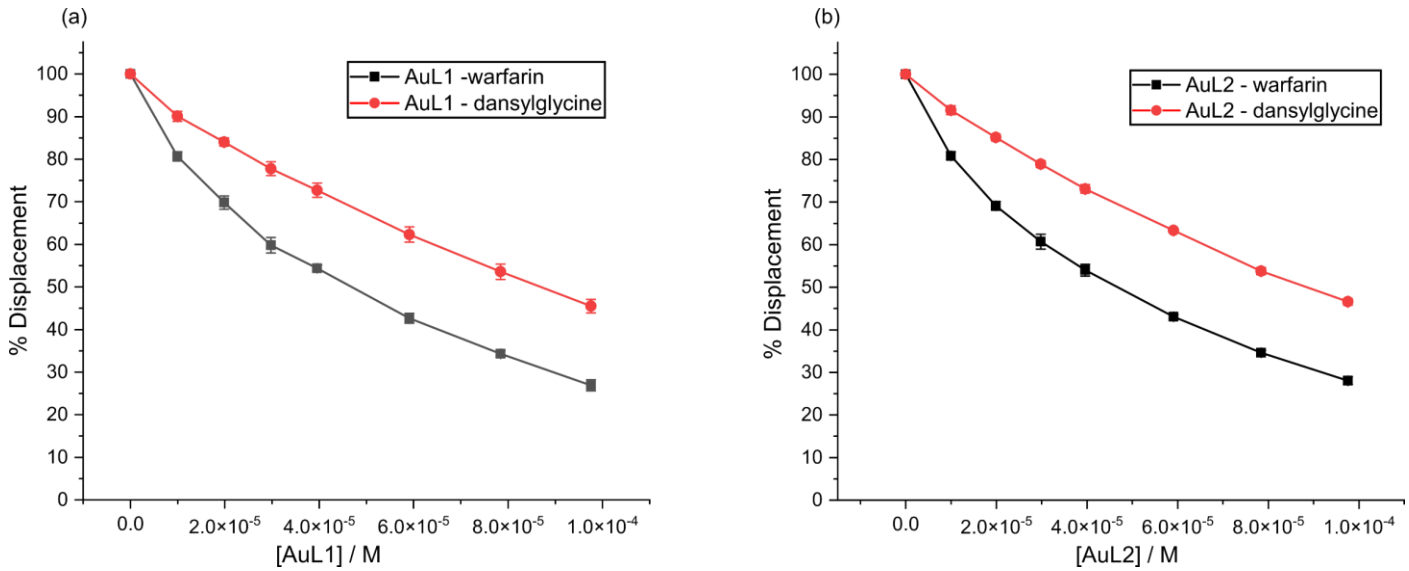

Fig. S23 AuL1 and **AuL2** displace either dansylglycine or warfarin bound to HSA. Various Au(III)-chelates (0 – 9.7 × 10^{-5} M) were titrated into a solution containing 5 μM HSA bound to 5 μM of either dansylglycine or warfarin. Displacement of dansylglycine or warfarin resulted in the fluorophores fluorescence being quenched. Error bars indicate the standard deviation of three independent experiments.

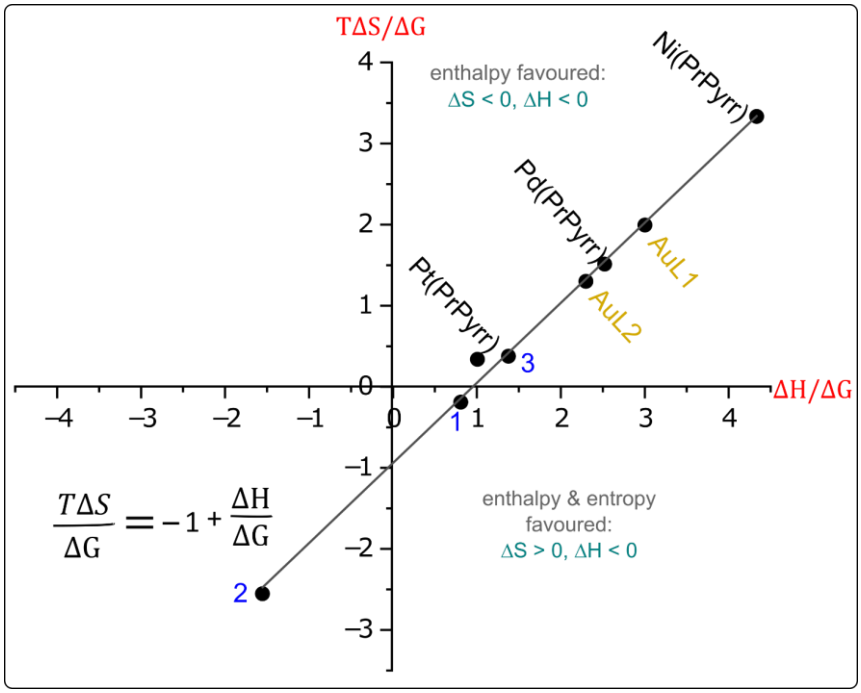

Fig. S24 Plot of the Gibbs-Helmholtz relationship (eq. 5) for the reaction of **AuL1** and **AuL2** with HSA at 298 K in 50 mM KH_2PO_4 buffer at pH 7.50 and six metal Schiff base chelates previously reported.[13,14] For all reactions, ΔG < 0. The same trend can be observed for Ni(PrPyrr) and Pd(PrPyrr) under varying pH's.[15]

2.3 CD spectroscopy data

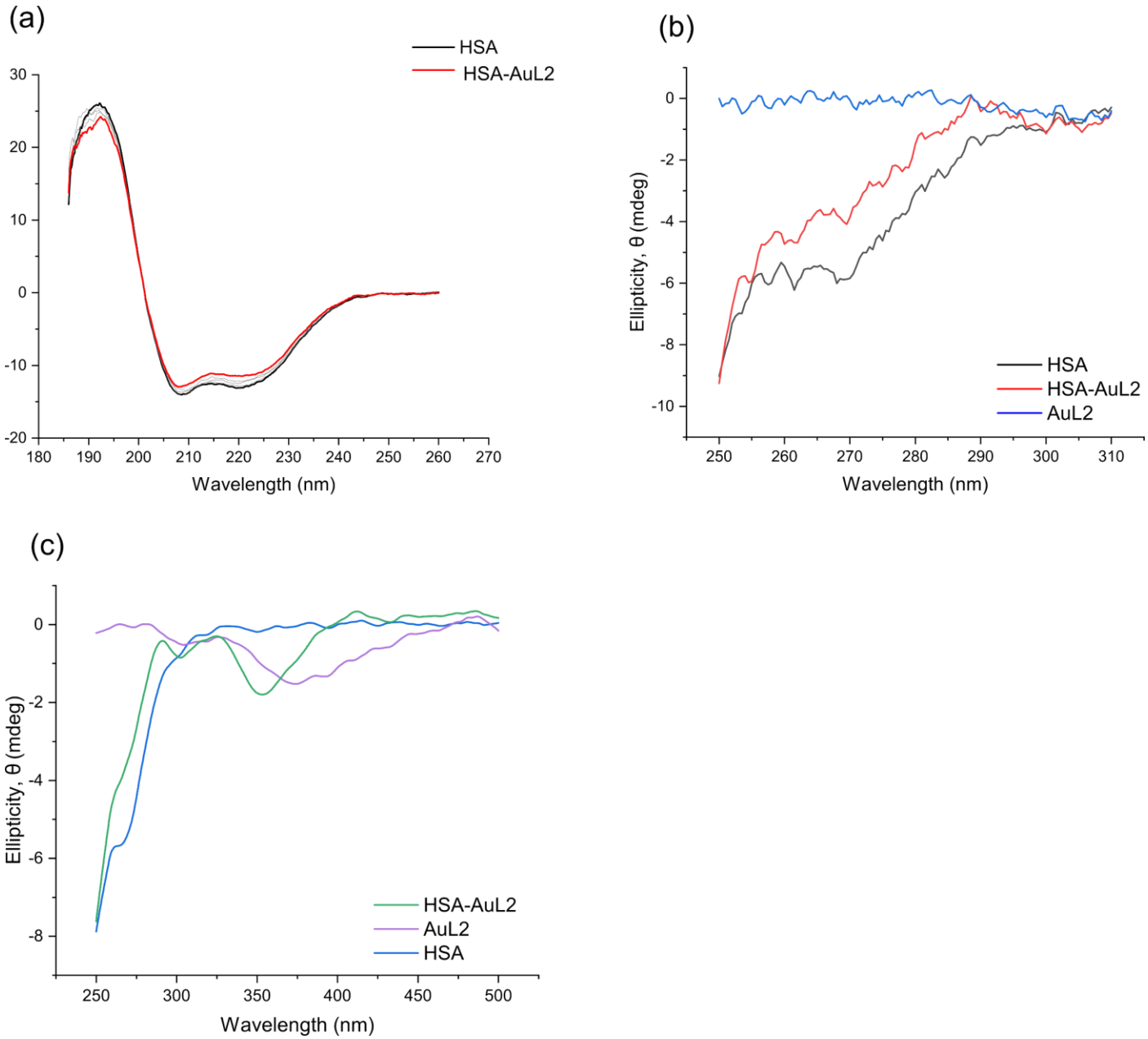

Fig. S25 (a) Far-UV CD spectra of native HAS (300 nM) and the protein incubated with saturating doses of **AuL2.** (b) near UV-visible CD spectra of native HSA (300 nM) and the protein incubated with a saturating dose (6 μM) of **AuL2**. (c) Represents the ICD spectrum of HSA in the presence of **AuL2**. The spectra were recorded at 298 K in 50 mM KH_2PO_4 buffer at pH 7.50 and ICD data was smoothed using a relatively fine Lowess function (0.07 span).

Table S1. Summary of the change in α-helicity of native and HSA in the presence of **AuL1** and **AuL2**.

Au(III) chelate	Concentration (µM)	% α–helicity
AuL1	0	58.96
	0.3	57.63
	1.5	56.90
	3	56.56
	6	56.36
AuL2	0	58.42
	0.3	58.75
	1.5	56.50
	3	56.22
	6	53.88

2.4 NCI-60 cytotoxicity data

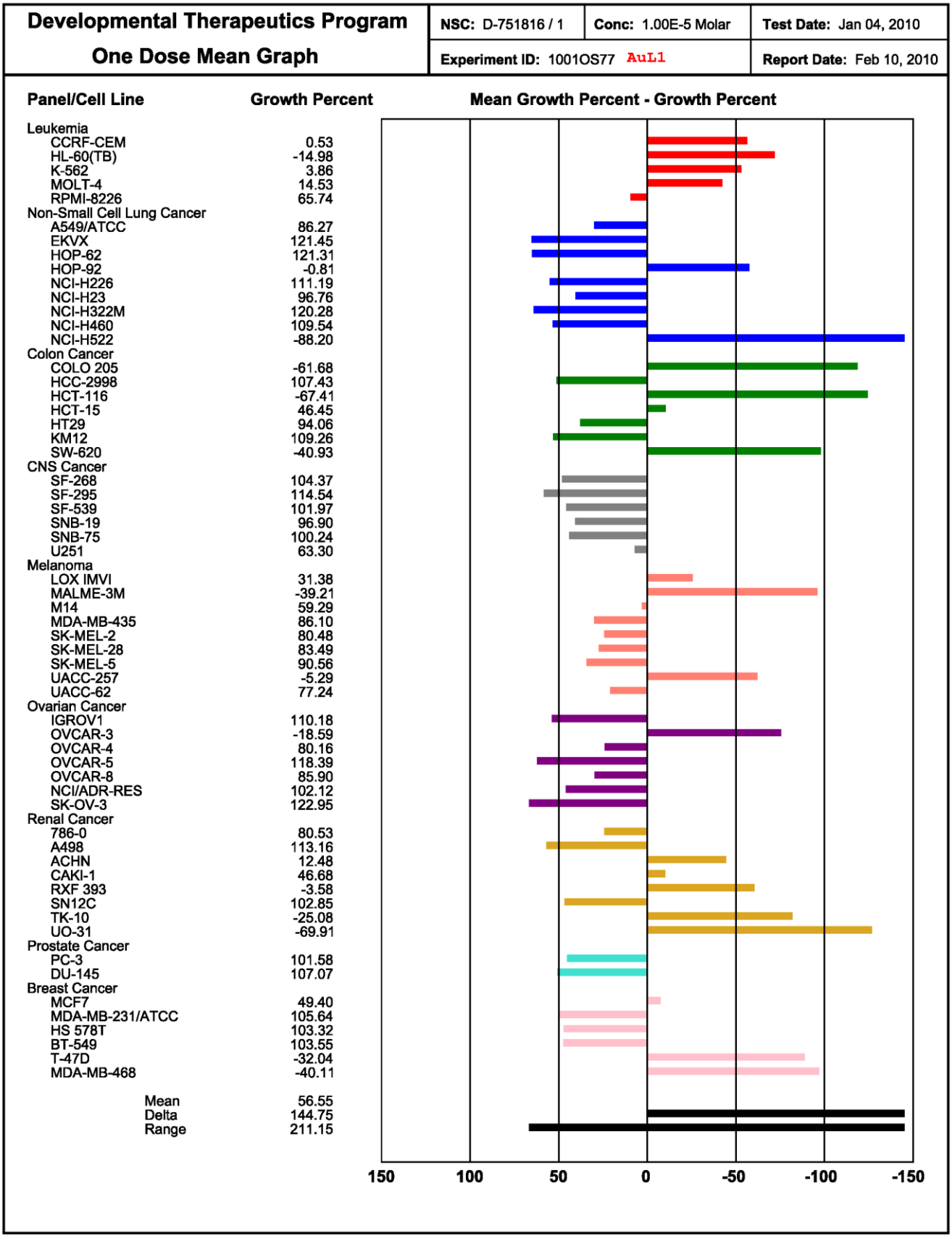

Fig. S26 NCI-60 single-dose cytotoxicity screen for **AuL1**.

Developmental Therapeutics Program

One Dose Mean Graph

NSC: D-751815 / 1	Conc: 1.00E-5 Molar	Test Date: Jan 04, 2010
Experiment ID: 1001OS77 AuL2 (1R,2R)		Report Date: Feb 10, 2010

Panel/Cell Line	Growth Percent
Leukemia	
CCRF-CEM	32.23
HL-60(TB)	76.01
K-562	28.06
MOLT-4	67.74
RPMI-8226	75.93
Non-Small Cell Lung Cancer	
A549/ATCC	99.77
EKVX	118.48
HOP-62	109.60
HOP-92	124.29
NCI-H226	118.87
NCI-H23	104.66
NCI-H322M	116.67
NCI-H460	107.79
NCI-H522	-90.27
Colon Cancer	
COLO 205	-13.93
HCC-2998	101.46
HCT-116	80.41
HCT-15	103.05
HT29	102.48
KM12	109.74
SW-620	40.87
CNS Cancer	
SF-268	96.65
SF-295	122.51
SF-539	103.84
SNB-19	99.81
SNB-75	108.18
U251	85.58
Melanoma	
LOX IMVI	48.88
MALME-3M	43.77
M14	79.24
MDA-MB-435	98.55
SK-MEL-2	95.09
SK-MEL-28	101.72
SK-MEL-5	99.05
UACC-257	81.97
UACC-62	86.74
Ovarian Cancer	
IGROV1	122.95
OVCAR-3	98.11
OVCAR-4	99.27
OVCAR-5	120.10
OVCAR-8	99.97
NCI/ADR-RES	102.65
SK-OV-3	122.08
Renal Cancer	
786-0	108.12
A498	114.06
ACHN	99.83
CAKI-1	105.68
RXF 393	66.12
SN12C	100.68
TK-10	85.44
UO-31	94.98
Prostate Cancer	
PC-3	98.42
DU-145	109.98
Breast Cancer	
MCF7	89.59
MDA-MB-231/ATCC	114.76
HS 578T	117.07
BT-549	111.61
T-47D	52.14
MDA-MB-468	58.50
Mean	89.11
Delta	179.38
Range	214.56

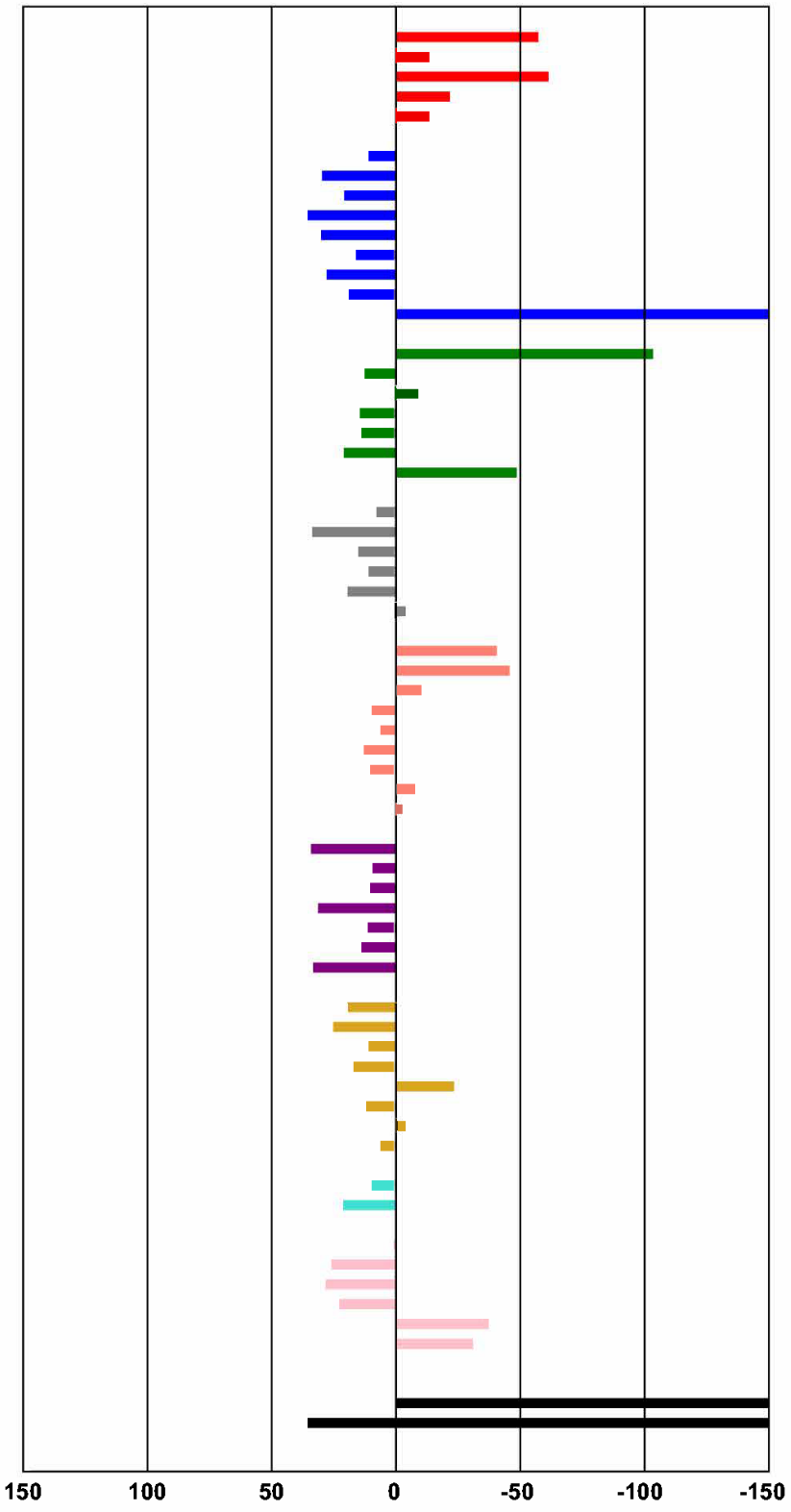

Fig. S27 NCI-60 single-dose cytotoxicity screen for **AuL2**.

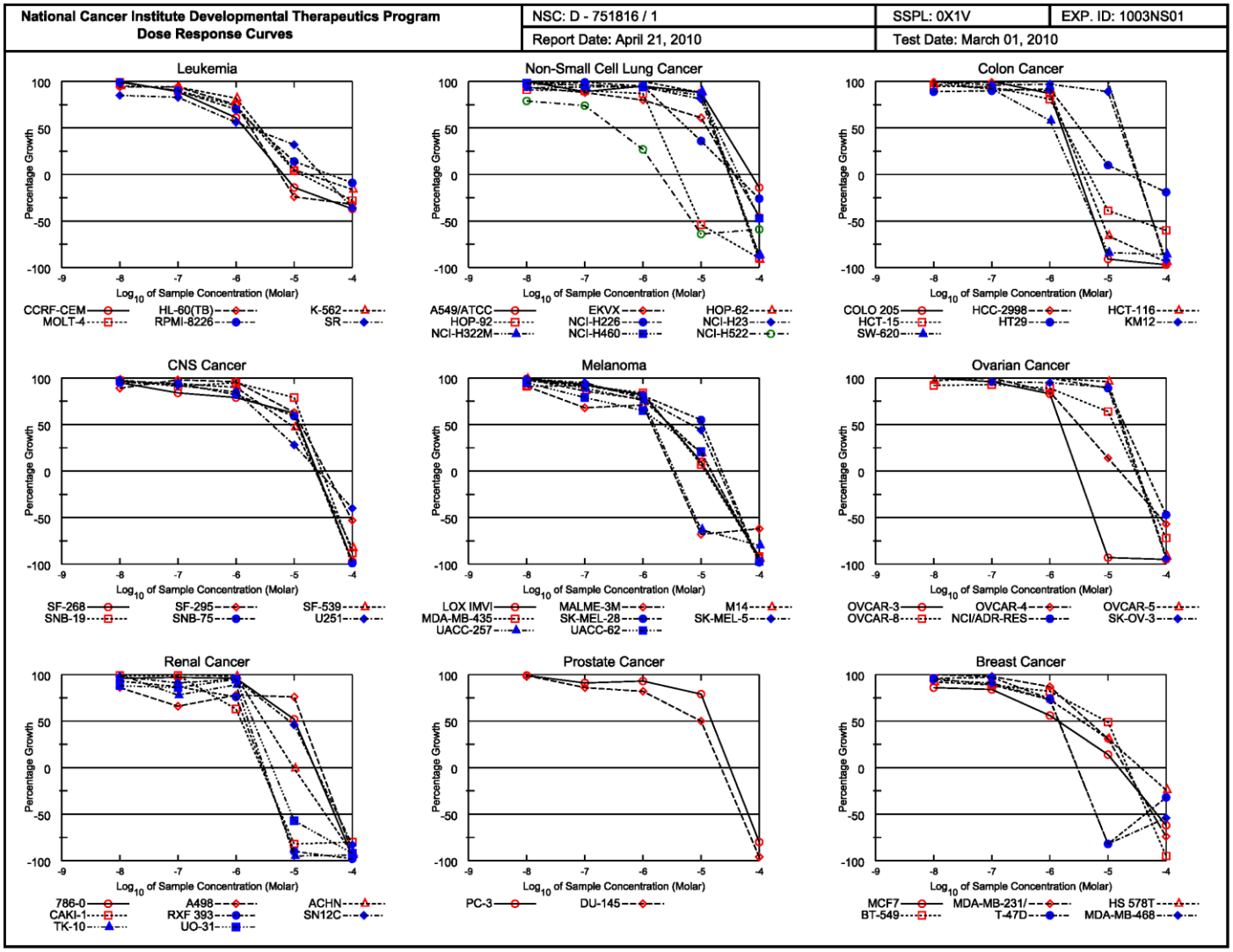

Fig. S28 NCI-60 five-dose cytotoxicity screen MTT assay graphs for **AuL1** with the panel of nine human cancer cell lines.

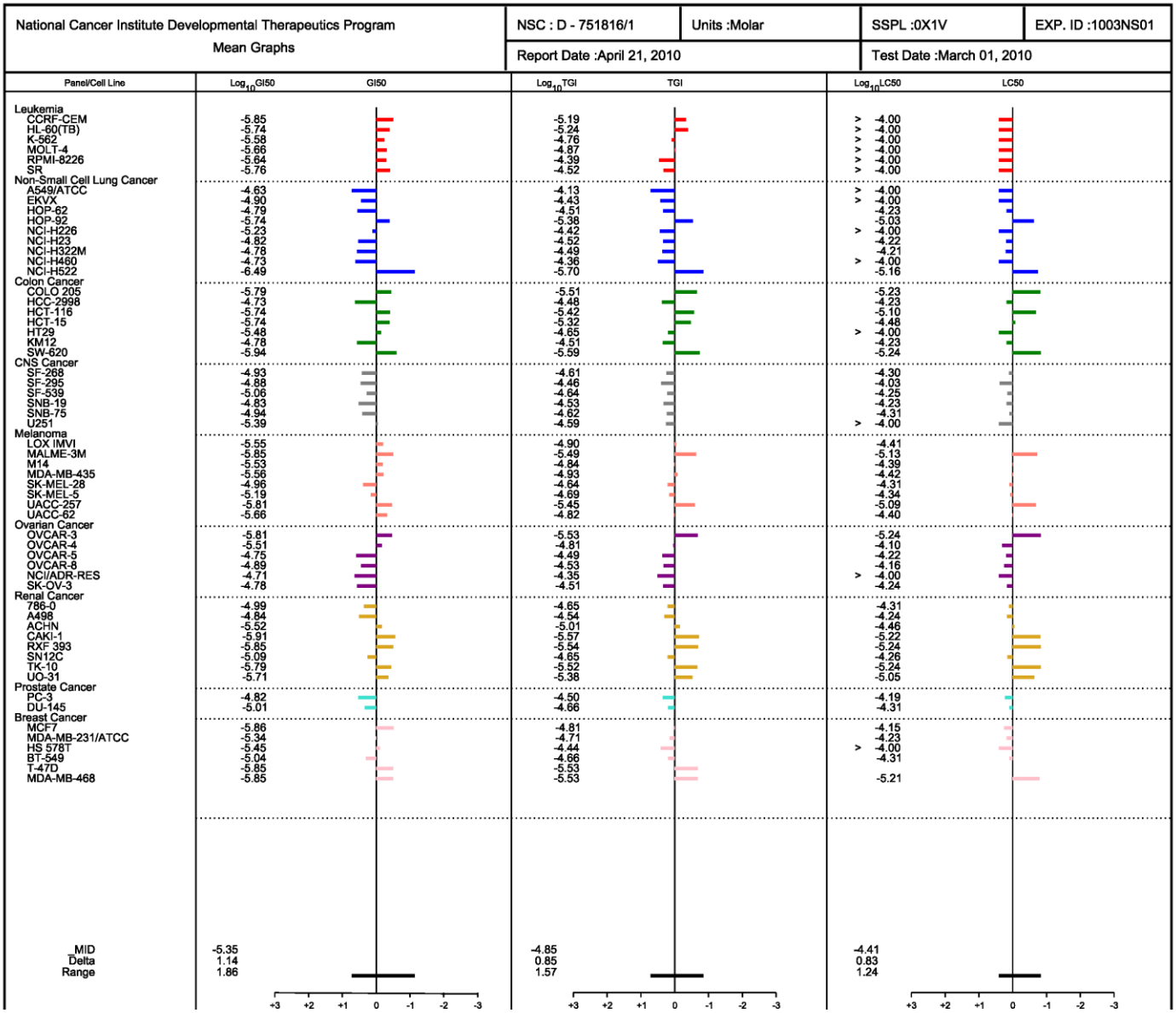

Fig. S29 NCI-60 five-dose cytotoxicity screen mean efficacy graphs for **AuL1**.

2.5 X-ray crystal structures

Table S2. Crystal system data, X-ray data collection, and structure refinement details for **AuL1**.

Identification code	19OA_SS_Au_CyHex_1S2S_0m
Empirical formula	$C_{16}H_{18}AuF_6N_4P$
Formula weight	608.28
Temperature/K	173.15
Crystal system	monoclinic
Space group	$P2_1$
a/Å	10.1292(3)
b/Å	9.7663(3)
c/Å	18.4954(6)
α/°	90
β/°	94.364(2)
γ/°	90
Volume/Å^3	1824.35(10)
Z	4
ρ_{calc}g/cm^3	2.215
μ/mm^{-1}	8.220
F(000)	1160.0
Crystal size/mm^3	0.282 × 0.125 × 0.093
Radiation	MoKα (λ = 0.71073)
2Θ range for data collection/°	2.208 to 59.342
Index ranges	-14 ≤ h ≤ 13, -13 ≤ k ≤ 13, -25 ≤ l ≤ 25
Reflections collected	28470
Independent reflections	10252 [R_{int} = 0.0277, R_{sigma} = 0.0449]
Data/restraints/parameters	10252/187/580
Goodness-of-fit on F^2	0.971
Final R indexes [I>=2σ (I)]	R_1 = 0.0258, wR_2 = 0.0427
Final R indexes [all data]	R_1 = 0.0362, wR_2 = 0.0449
Largest diff. peak/hole / e Å^{-3}	1.27/-0.73
Flack parameter	0.031(9)
CCDC Deposit Number	2244592

Table S3. Bond lengths for **AuL1**.

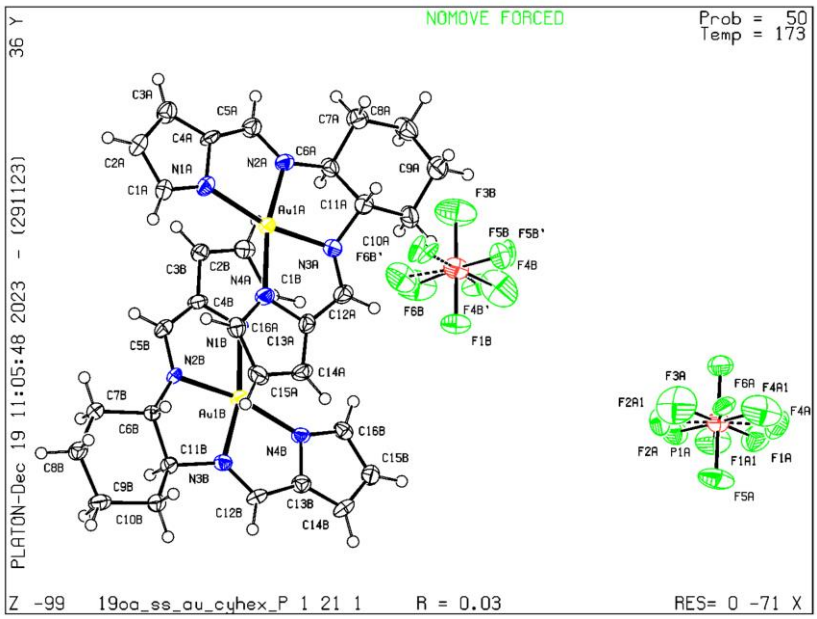

Atom	Atom	Length/Å		Atom	Atom	Length/Å
Au1B	N1B	2.026(6)		N4A	C13A	1.414(9)
Au1B	N2B	1.983(6)		N4A	C16A	1.339(11)
Au1B	N3B	1.979(6)		C1A	C2A	1.382(11)
Au1B	N4B	1.996(6)		C2A	C3A	1.394(13)
N1B	C1B	1.342(11)		C3A	C4A	1.409(11)
N1B	C4B	1.373(9)		C4A	C5A	1.378(11)
N2B	C5B	1.313(10)		C6A	C7A	1.524(10)
N2B	C6B	1.472(9)		C6A	C11A	1.523(9)
N3B	C11B	1.492(8)		C7A	C8A	1.525(11)
N3B	C12B	1.302(9)		C8A	C9A	1.505(11)
N4B	C13B	1.403(11)		C9A	C10A	1.521(11)
N4B	C16B	1.348(10)		C10A	C11A	1.512(10)
C1B	C2B	1.365(11)		C12A	C13A	1.422(13)
C2B	C3B	1.389(11)		C13A	C14A	1.380(13)
C3B	C4B	1.407(12)		C14A	C15A	1.379(12)
C4B	C5B	1.398(13)		C15A	C16A	1.403(11)
C6B	C7B	1.524(9)		P1A	F6A	1.598(4)
C6B	C11B	1.530(8)		P1A	F3A	1.580(5)
C7B	C8B	1.562(11)		P1A	F5A	1.591(4)
C8B	C9B	1.525(9)		P1A	F1A	1.589(5)
C9B	C10B	1.535(11)		P1A	F4A	1.569(4)
C10B	C11B	1.515(11)		P1A	F2A	1.601(4)

Atom	Atom	Length/Å		Atom	Atom	Length/Å
C12B	C13B	1.424(11)		P1A	F2A1	1.588(6)
C13B	C14B	1.376(11)		P1A	F4A1	1.586(6)
C14B	C15B	1.380(12)		P1A	F1A1	1.581(6)
C15B	C16B	1.392(11)		P1A	F3A1	1.588(6)
Au1A	N1A	2.024(6)		P1B	F1B	1.601(4)
Au1A	N2A	1.980(7)		P1B	F2B	1.589(5)
Au1A	N3A	1.957(7)		P1B	F3B	1.596(4)
Au1A	N4A	1.999(7)		P1B	F4B	1.596(5)
N1A	C1A	1.327(11)		P1B	F5B	1.599(5)
N1A	C4A	1.392(12)		P1B	F6B	1.585(5)
N2A	C5A	1.292(9)		P1B	F4B'	1.587(5)
N2A	C6A	1.468(9)		P1B	F2B'	1.593(5)
N3A	C11A	1.491(9)		P1B	F5B'	1.594(5)
N3A	C12A	1.287(10)		P1B	F6B'	1.594(5)

Table S4. Bond angles for **AuL1**.

Atom	Atom	Atom	Angle/˚		Atom	Atom	Atom	Angle/˚
N2B	Au1B	N1B	81.3(3)		C9A	C8A	C7A	112.5(7)
N2B	Au1B	N4B	166.0(3)		C8A	C9A	C10A	112.3(6)
N3B	Au1B	N1B	165.8(2)		C11A	C10A	C9A	106.7(6)
N3B	Au1B	N2B	84.6(3)		N3A	C11A	C6A	106.7(5)
N3B	Au1B	N4B	81.4(3)		N3A	C11A	C10A	115.3(6)
N4B	Au1B	N1B	112.7(3)		C10A	C11A	C6A	111.7(6)
C1B	N1B	Au1B	141.2(6)		N3A	C12A	C13A	116.9(7)
C1B	N1B	C4B	108.5(7)		N4A	C13A	C12A	113.7(7)
C4B	N1B	Au1B	110.3(6)		C14A	C13A	N4A	108.2(8)
C5B	N2B	Au1B	114.7(6)		C14A	C13A	C12A	137.9(8)
C5B	N2B	C6B	131.6(7)		C15A	C14A	C13A	107.9(7)
C6B	N2B	Au1B	112.5(4)		C14A	C15A	C16A	106.9(8)
C11B	N3B	Au1B	111.3(4)		N4A	C16A	C15A	110.0(7)
C12B	N3B	Au1B	115.0(6)		F6A	P1A	F2A	88.8(3)
C12B	N3B	C11B	131.9(6)		F3A	P1A	F6A	88.1(4)
C13B	N4B	Au1B	112.3(6)		F3A	P1A	F5A	92.8(4)
C16B	N4B	Au1B	141.7(6)		F3A	P1A	F1A	174.6(5)
C16B	N4B	C13B	106.0(6)		F3A	P1A	F2A	88.3(5)
N1B	C1B	C2B	109.3(8)		F5A	P1A	F6A	179.0(3)
C1B	C2B	C3B	108.4(8)		F5A	P1A	F2A	90.8(3)
C2B	C3B	C4B	105.8(7)		F1A	P1A	F6A	89.7(4)
N1B	C4B	C3B	107.9(8)		F1A	P1A	F5A	89.4(4)

Atom	Atom	Atom	Angle/˚		Atom	Atom	Atom	Angle/˚
N1B	C4B	C5B	117.5(7)		F1A	P1A	F2A	86.7(4)
C5B	C4B	C3B	134.6(7)		F4A	P1A	F6A	89.7(4)
N2B	C5B	C4B	116.2(7)		F4A	P1A	F3A	92.7(6)
N2B	C6B	C7B	114.4(6)		F4A	P1A	F5A	90.7(4)
N2B	C6B	C11B	109.2(5)		F4A	P1A	F1A	92.3(6)
C7B	C6B	C11B	110.1(5)		F4A	P1A	F2A	178.2(6)
C6B	C7B	C8B	108.0(6)		F2A1	P1A	F6A	95.0(10)
C9B	C8B	C7B	112.2(6)		F2A1	P1A	F5A	85.5(10)
C8B	C9B	C10B	114.3(6)		F4A1	P1A	F6A	89.9(11)
C11B	C10B	C9B	107.3(7)		F4A1	P1A	F5A	89.8(11)
N3B	C11B	C6B	108.2(5)		F4A1	P1A	F2A1	170.9(17)
N3B	C11B	C10B	115.0(6)		F4A1	P1A	F3A1	85.0(15)
C10B	C11B	C6B	110.2(6)		F1A1	P1A	F6A	89.8(11)
N3B	C12B	C13B	117.4(8)		F1A1	P1A	F5A	89.3(11)
N4B	C13B	C12B	113.8(7)		F1A1	P1A	F2A1	93.6(17)
C14B	C13B	N4B	109.2(8)		F1A1	P1A	F4A1	94.1(18)
C14B	C13B	C12B	136.6(8)		F1A1	P1A	F3A1	177.2(14)
C13B	C14B	C15B	107.3(8)		F3A1	P1A	F6A	92.8(9)
C14B	C15B	C16B	107.0(8)		F3A1	P1A	F5A	88.1(9)
N4B	C16B	C15B	110.4(8)		F3A1	P1A	F2A1	87.2(15)
N2A	Au1A	N1A	81.7(3)		F2B	P1B	F1B	92.8(8)
N2A	Au1A	N4A	165.1(3)		F2B	P1B	F3B	85.6(8)
N3A	Au1A	N1A	165.7(3)		F2B	P1B	F4B	174.9(7)
N3A	Au1A	N2A	84.2(3)		F2B	P1B	F5B	89.3(7)
N3A	Au1A	N4A	81.3(3)		F3B	P1B	F1B	178.3(3)
N4A	Au1A	N1A	113.0(3)		F3B	P1B	F4B	96.2(7)
C1A	N1A	Au1A	140.9(7)		F3B	P1B	F5B	92.0(7)
C1A	N1A	C4A	110.1(6)		F4B	P1B	F1B	85.4(7)
C4A	N1A	Au1A	109.0(6)		F4B	P1B	F5B	85.9(7)
C5A	N2A	Au1A	114.3(6)		F5B	P1B	F1B	87.4(7)
C5A	N2A	C6A	133.2(7)		F6B	P1B	F1B	89.0(7)
C6A	N2A	Au1A	111.9(4)		F6B	P1B	F2B	94.4(9)
C11A	N3A	Au1A	110.7(4)		F6B	P1B	F3B	91.7(7)
C12A	N3A	Au1A	116.4(6)		F6B	P1B	F4B	90.3(7)
C12A	N3A	C11A	131.7(7)		F6B	P1B	F5B	175.0(9)
C13A	N4A	Au1A	111.5(6)		F4B'	P1B	F1B	94.3(7)
C16A	N4A	Au1A	141.6(6)		F4B'	P1B	F3B	87.4(7)
C16A	N4A	C13A	106.9(7)		F4B'	P1B	F2B'	173.6(11)
N1A	C1A	C2A	109.5(8)		F4B'	P1B	F5B'	95.5(11)
C1A	C2A	C3A	106.9(8)		F4B'	P1B	F6B'	89.3(10)
C2A	C3A	C4A	107.9(8)		F2B'	P1B	F1B	85.1(9)

Atom	Atom	Atom	Angle/˚		Atom	Atom	Atom	Angle/˚
N1A	C4A	C3A	105.7(8)		F2B'	P1B	F3B	93.2(9)
C5A	C4A	N1A	117.5(7)		F2B'	P1B	F5B'	91.0(11)
C5A	C4A	C3A	136.8(8)		F2B'	P1B	F6B'	84.3(10)
N2A	C5A	C4A	117.5(8)		F5B'	P1B	F1B	95.3(11)
N2A	C6A	C7A	115.0(5)		F5B'	P1B	F3B	84.5(11)
N2A	C6A	C11A	107.3(6)		F6B'	P1B	F1B	88.9(9)
C11A	C6A	C7A	110.2(6)		F6B'	P1B	F3B	91.1(9)
C6A	C7A	C8A	110.6(6)		F6B'	P1B	F5B'	173.3(13)

Table S5. Crystal system data, X-ray data collection, and structure refinement details for **AuL2**.

Identification code	Au1R2RL2PF6
Empirical formula	$C_{16}H_{18}AuF_6N_4P$
Formula weight	608.279
Temperature/K	100.15
Crystal system	orthorhombic
Space group	$P2_122_1$
a/Å	10.3951(2)
b/Å	18.2575(3)
c/Å	10.0206(2)
α/°	90
β/°	90
γ/°	90
Volume/Å^3	1901.80(6)
Z	4
ρ_{calc}g/cm^3	2.124
μ/mm^{-1}	7.886
F(000)	1155.5
Crystal size/mm^3	0.6 × 0.2 × 0.1
Radiation	Mo Kα (λ = 0.71073)
2Θ range for data collection/°	5.94 to 68.52
Index ranges	-15 ≤ h ≤ 15, -28 ≤ k ≤ 28, -15 ≤ l ≤ 13
Reflections collected	30977
Independent reflections	7216 [R_{int} = 0.0730, R_{sigma} = 0.0401]
Data/restraints/parameters	7216/0/255
Goodness-of-fit on F^2	1.046
Final R indexes [I>=2σ (I)]	R_1 = 0.0456, wR_2 = 0.1300
Final R indexes [all data]	R_1 = 0.0548, wR_2 = 0.1433
Largest diff. peak/hole / e Å^{-3}	3.78/-3.90
Flack parameter	-0.006(10)
CCDC Deposit Number	2244999

Table S6. Bond lengths for **AuL2**.

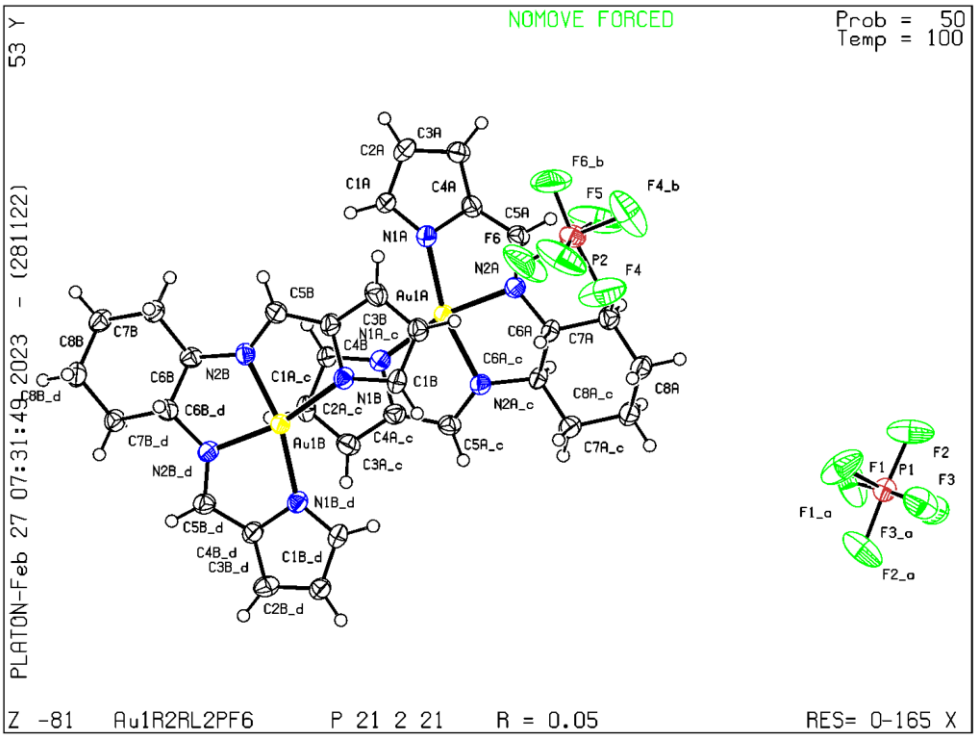

Atom	Atom	Length/Å		Atom	Atom	Length/Å
Au_{1A}	N_{1A}	2.014(4)		Au_{1B}	N_{2B}	1.970(4)
Au_{1A}	$N_{1A}{}^{1}$	2.014(4)		C_{1B}	C_{2B}	1.408(8)
Au_{1A}	$N_{2A}{}^{1}$	1.982(4)		C_{1B}	N_{1B}	1.346(5)
Au_{1A}	N_{2A}	1.982(4)		C_{2B}	C_{3B}	1.389(8)
C_{1A}	C_{2A}	1.412(8)		C_{3B}	C_{4B}	1.398(8)
C_{1A}	N_{1A}	1.349(5)		C_{4B}	C_{5B}	1.423(7)
C_{2A}	C_{3A}	1.391(7)		C_{4B}	N_{1B}	1.388(7)
C_{3A}	C_{4A}	1.403(8)		C_{5B}	N_{2B}	1.322(6)
C_{4A}	C_{5A}	1.415(7)		C_{6B}	$C_{6B}{}^{2}$	1.516(9)
C_{4A}	N_{1A}	1.393(7)		C_{6B}	C_{7B}	1.523(6)
C_{5A}	N_{2A}	1.304(6)		C_{6B}	N_{2B}	1.477(6)
C_{6A}	$C_{6A}{}^{1}$	1.552(9)		C_{7B}	C_{8B}	1.533(7)
C_{6A}	C_{7A}	1.511(6)		C_{8B}	$C_{8B}{}^{2}$	1.529(11)
C_{6A}	N_{2A}	1.463(6)		F_1	P_1	1.562(4)
C_{7A}	C_{8A}	1.530(7)		F_2	$P_1{}^{1}$	1.600(4)
C_{8A}	$C_{8A}{}^{1}$	1.528(11)		F_3	P_1	1.609(4)
Au_{1B}	$N_{1B}{}^{2}$	2.007(4)		F_4	P_2	1.614(5)
Au_{1B}	N_{1B}	2.007(4)		F_5	$P_2{}^{3}$	1.580(5)
Au_{1B}	$N_{2B}{}^{2}$	1.970(4)		F_6	P_2	1.518(5)

[1]1-X,+Y,1-Z; [2]1-X,+Y,-Z; [3]2-X,+Y,1-Z

Table S7. Bond lengths for **AuL2**.

Atom	Atom	Atom	Angle/˚		Atom	Atom	Atom	Angle/˚
N_{1A}	Au_{1A}	N_{1A}^{1}	113.2(2)		C_{8B}^{2}	C_{8B}	C_{7B}	111.7(4)
N_{2A}^{1}	Au_{1A}	N_{1A}	164.75(17)		C_{1B}	N_{1B}	Au_{1B}	141.3(4)
N_{2A}^{1}	Au_{1A}	N_{1A}^{1}	81.65(15)		C_{4B}	N_{1B}	Au_{1B}	111.3(3)
N_{2A}	Au_{1A}	N_{1A}	81.65(15)		C_{4B}	N_{1B}	C_{1B}	107.3(4)
N_{2A}	Au_{1A}	N_{1A}^{1}	164.75(17)		C_{5B}	N_{2B}	Au_{1B}	115.6(3)
N_{2A}	Au_{1A}	N_{2A}^{1}	83.7(2)		C_{6B}	N_{2B}	Au_{1B}	112.2(3)
N_{1A}	C_{1A}	C_{2A}	108.3(4)		C_{6B}	N_{2B}	C_{5B}	131.0(4)
C_{3A}	C_{2A}	C_{1A}	107.9(5)		F_1^{1}	P_1	F_1	96.2(5)
C_{4A}	C_{3A}	C_{2A}	106.8(5)		F_2^{1}	P_1	F_1	93.6(3)
C_{5A}	C_{4A}	C_{3A}	135.9(5)		F_2^{1}	P_1	F_1^{1}	88.5(3)
N_{1A}	C_{4A}	C_{3A}	108.1(5)		F_2	P_1	F_1	88.5(3)
N_{1A}	C_{4A}	C_{5A}	116.0(5)		F_2	P_1	F_1^{1}	93.6(3)
N_{2A}	C_{5A}	C_{4A}	116.6(5)		F_2	P_1	F_2^{1}	176.8(5)
N_{2A}	C_{6A}	C_{7A}	116.0(4)		F_3^{1}	P_1	F_1	174.7(3)
C_{8A}	C_{7A}	C_{6A}	110.0(4)		F_3^{1}	P_1	F_1^{1}	87.5(3)
C_{8A}^{1}	C_{8A}	C_{7A}	111.4(4)		F_3	P_1	F_1^{1}	174.7(3)
C_{1A}	N_{1A}	Au_{1A}^{1}	140.2(4)		F_3	P_1	F_1	87.5(3)
C_{4A}	N_{1A}	Au_{1A}^{1}	110.7(3)		F_3	P_1	F_2^{1}	87.5(2)
C_{4A}	N_{1A}	C_{1A}	108.9(4)		F_3^{1}	P_1	F_2^{1}	90.2(2)
C_{5A}	N_{2A}	Au_{1A}^{1}	114.9(3)		F_3	P_1	F_2	90.2(2)
C_{6A}	N_{2A}	Au_{1A}^{1}	111.5(3)		F_3^{1}	P_1	F_2	87.5(2)
C_{6A}	N_{2A}	C_{5A}	132.7(4)		F_3^{1}	P_1	F_3	89.1(4)
N_{1B}^{2}	Au_{1B}	N_{1B}	113.0(2)		F_4^{3}	P_2	F_4	87.2(5)
N_{2B}	Au_{1B}	N_{1B}	81.63(15)		F_5^{3}	P_2	F_4^{3}	86.5(3)
N_{2B}^{2}	Au_{1B}	N_{1B}	165.36(17)		F_5^{3}	P_2	F_4	84.8(3)
N_{2B}^{2}	Au_{1B}	N_{1B}^{2}	81.63(15)		F_5	P_2	F_4	86.5(3)
N_{2B}	Au_{1B}	N_{1B}^{2}	165.36(17)		F_5	P_2	F_4^{3}	84.8(3)
N_{2B}^{2}	Au_{1B}	N_{2B}	83.8(2)		F_5	P_2	F_5^{3}	167.8(6)
N_{1B}	C_{1B}	C_{2B}	109.7(4)		F_6^{3}	P_2	F_4^{3}	85.0(4)
C_{3B}	C_{2B}	C_{1B}	107.2(5)		F_6	P_2	F_4	85.0(4)
C_{4B}	C_{3B}	C_{2B}	106.5(6)		F_6	P_2	F_4^{3}	171.9(4)
C_{5B}	C_{4B}	C_{3B}	134.5(6)		F_6^{3}	P_2	F_4	171.9(4)
N_{1B}	C_{4B}	C_{3B}	109.3(5)		F_6^{3}	P_2	F_5	95.2(4)
N_{1B}	C_{4B}	C_{5B}	116.1(5)		F_6	P_2	F_5	92.4(4)
N_{2B}	C_{5B}	C_{4B}	115.3(5)		F_6^{3}	P_2	F_5^{3}	92.4(4)
N_{2B}	C_{6B}	C_{7B}	115.8(4)		F_6	P_2	F_5^{3}	95.2(4)
C_{8B}	C_{7B}	C_{6B}	108.9(4)		F_6^{3}	P_2	F_6	102.8(6)

[1]1-X,+Y,1-Z; [2]1-X,+Y,-Z; [3]2-X,+Y,1-Z

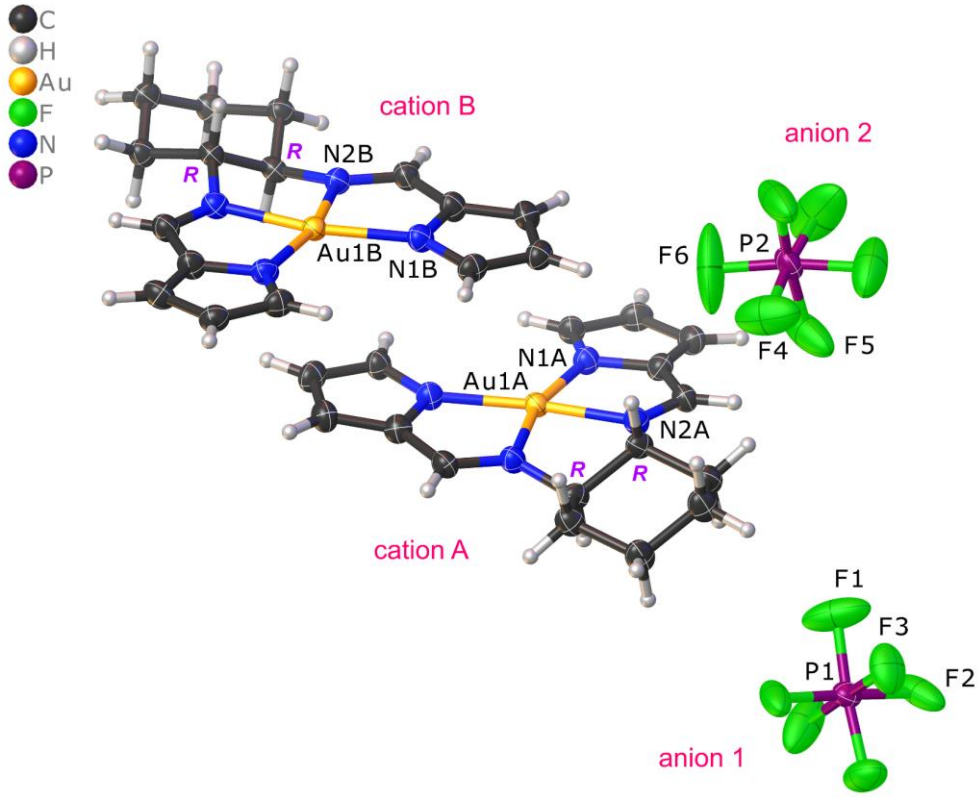

Fig. S30 Partly labelled low-temperature X-ray structure of **AuL2** (*R,R*-enantiomer, 50% thermal ellipsoids) depicting the complete ion pairs A and B. Each cation and anion for **AuL2** is located on a 2-fold axis passing through the Au(III) ion or the P atom of the anion. The cation pair geometry suggests π-π stacking interactions are operative.

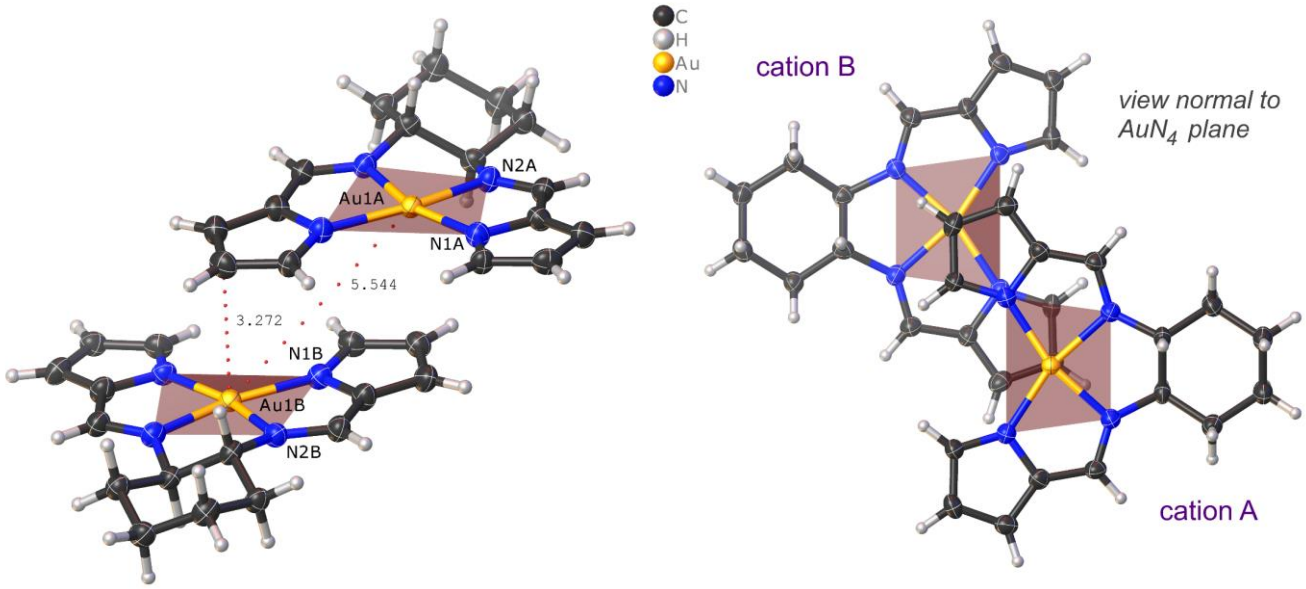

Fig. S31 Illustration of the π-π stacking geometry between independent cation pairs within the lattice of **AuL2**. The interaction distances are in Å. Note how the Au(III) ions interact axially with a pyrrole β-C atom.

Table S8. Selected bond lengths (Å) and bond angles (°) for **AuL1** and **AuL2**. Within error, chemically unique bond distances and bond angles are equivalent for the two enantiomers.

AuL1 (1S,2S)*

Au-N_{imine}	Au-$N_{pyrrole}$	C=N imine	N_{im}-Au-N_{im}	N_p-Au-N_p	cis-N_p-Au-N_{im}	trans-N_p-Au-N_{im}	C_p-C_{im}-N_{im}
1.983	2.026	1.302	84.6	112.7	81.37	165.8	117.5
1.979	1.996	1.313	84.2	113.0	81.20	166.0	116.2
1.980	2.024	1.287			81.35	165.1	115.0
1.957	1.999	1.292			81.69	165.7	117.5
AVE: 1.975	2.011	1.299	84.4	112.9	81.4	165.7	116.6
ESD: 0.012	0.016	0.012	0.3	0.2	0.2	0.4	1.2

AuL2 (1R,2R)**

Au-N_{imine}	Au-$N_{pyrrole}$	C=N imine	N_{im}-Au-N_{im}	N_p-Au-N_p	cis-N_p-Au-N_{im}	trans-N_p-Au-N_{im}	C_p-C_{im}-N_{im}
1.970	2.007	1.322	83.79	112.97	81.63	165.39	116.67
1.970	2.007	1.322	83.72	113.22	81.63	165.39	116.67
1.986	2.014	1.304			81.66	164.76	115.23
1.986	2.014	1.304			81.66	164.76	115.23
AVE: 1.978	2.011	1.313	83.8	113.1	81.6	165.1	116.0
ESD: 0.009	0.004	0.010	0.0	0.2	0.0	0.4	0.8

*There are two independent full molecules in the ASU. **There are two independent half-molecules in the ASU.

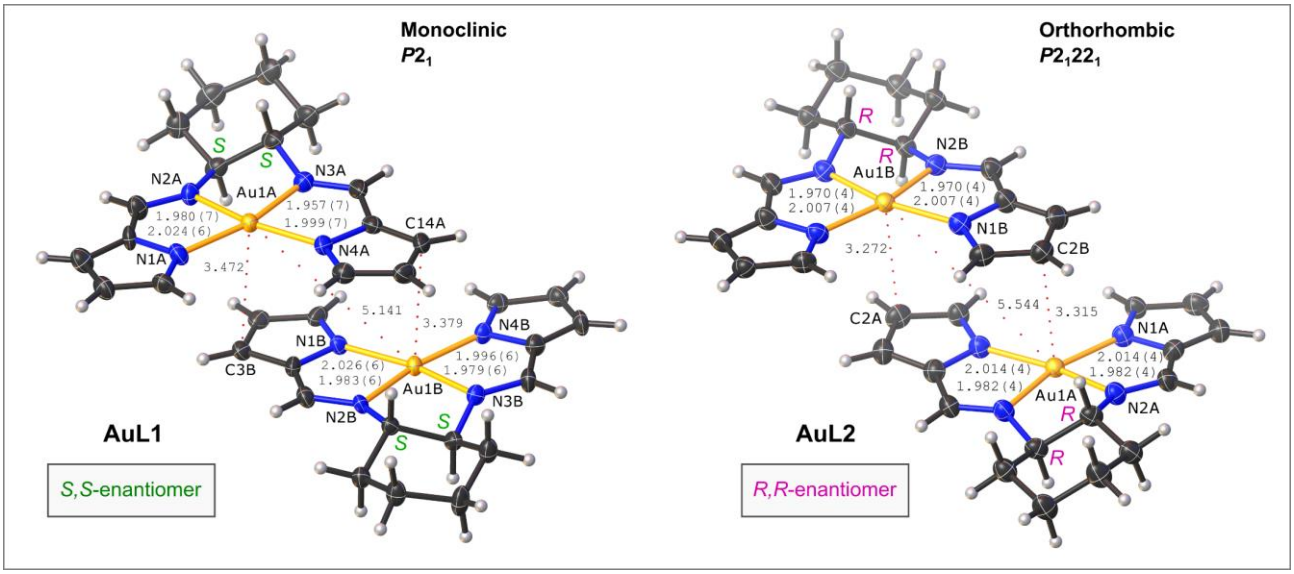

Fig. S32 Comparison of the low-temperature X-ray structures of the cation pairs formed by **AuL1** (*S,S*-enantiomer) and **AuL2** (*R,R*-enantiomer). Each cation for **AuL2** is located on a 2-fold axis passing through the Au(III) ion. Similar π-stacking is evident for both cation pairs, however, the cation pair for **AuL1** is somewhat more closely interacting, as evidenced by the shorter Au···Au and Au···C(pyrrole) nonbonded distances. All bond and interaction distances are in Å. Thermal ellipsoids are rendered at the 50% probability level.

2.6 GSH reacting with AuL1

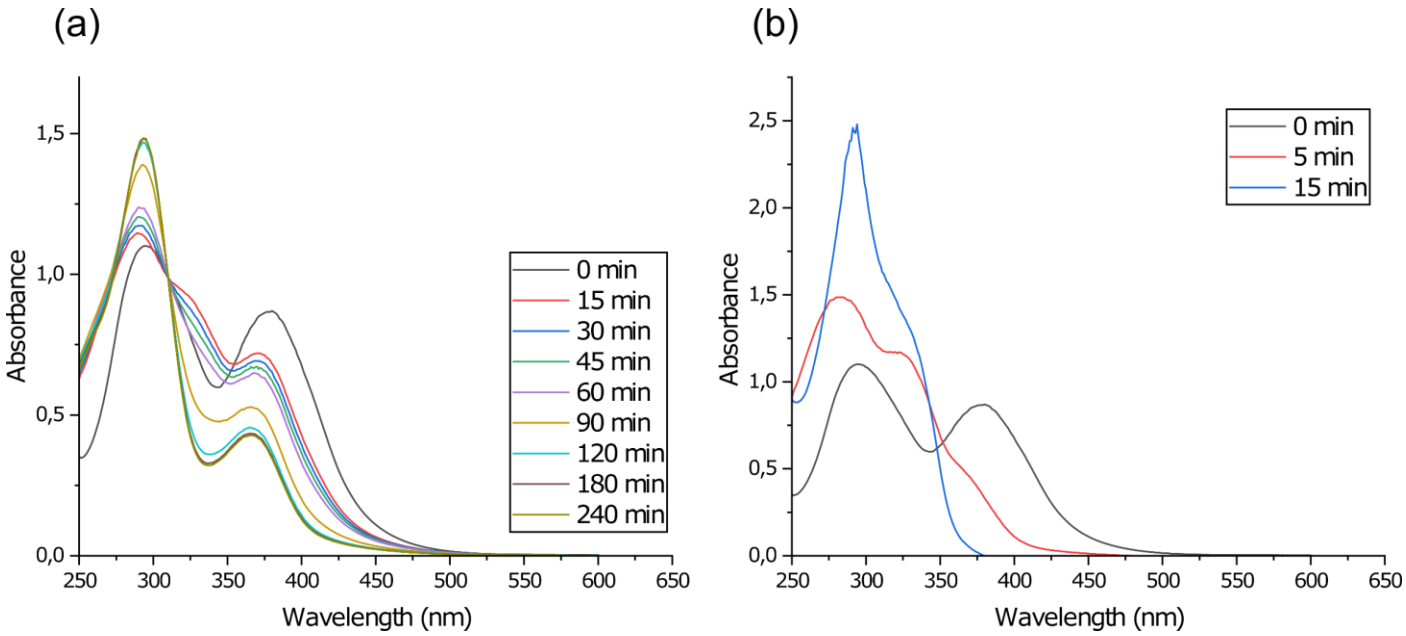

Fig. S33 Electronic absorption spectra of 100 μM **AuL1** in KH_2PO_4 buffer (50 mM; pH 7.5) (10% V/V) and DMSO mixture containing GSH (a) at a molar ratio of 1 :1 [**AuL1**]:[GSH] (b) at a molar ratio of 1:10 [**AuL1**]:[GSH].

2.7 The reaction of AuL1 with ctDNA

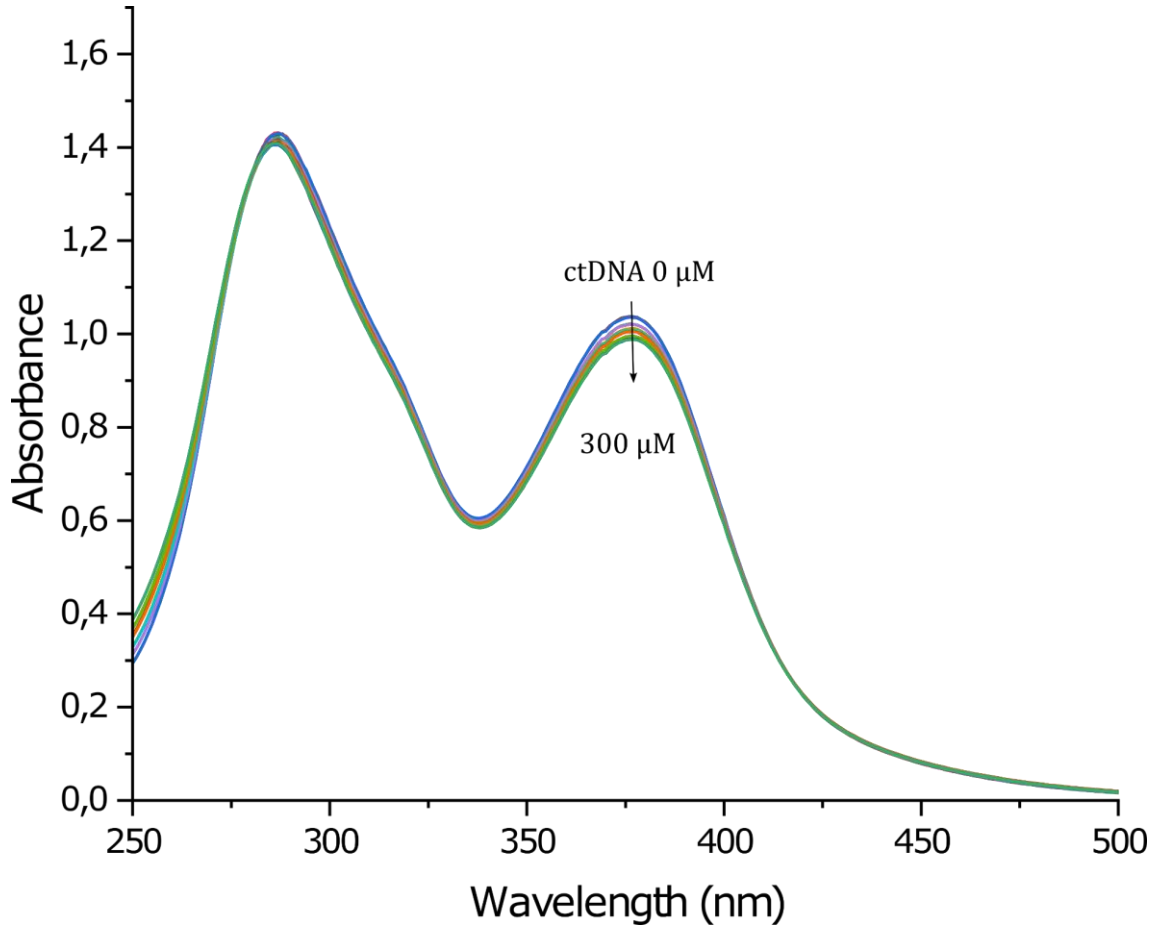

Fig. S34 (a) The UV-vis absorption spectra of **AuL1** representimg the change in the absorbance as a function of [ctDNA] fitted. The reaction was carried out in KH_2PO_4 and after sequential additions of ctDNA (final [ctDNA] = 300 µM bp, for **AuL1**.

Caveat. The minimal change in the electronic spectrum of **AuL1** with the addition of ctDNA indicate that **AuL1** does not bind to ctDNA.

3. References

1 O. V. Dolomanov, L. J. Bourhis, R. J. Gildea, J. a. K. Howard and H. Puschmann, *J. Appl. Crystallogr.*, 2009, **42**, 339–341.

2 G. M. Sheldrick, *Acta Crystallogr. Sect. Found. Adv.*, 2015, **71**, 3–8.

3 G. M. Sheldrick, *Acta Crystallogr. Sect. C Struct. Chem.*, 2015, **71**, 3–8.

4 F. Kleemiss, O. V. Dolomanov, M. Bodensteiner, N. Peyerimhoff, L. Midgley, L. J. Bourhis, A. Genoni, L. A. Malaspina, D. Jayatilaka, J. L. Spencer, F. White, B. Grundkötter-Stock, S. Steinhauer, D. Lentz, H. Puschmann and S. Grabowsky, *Chem. Sci.*, 2021, **12**, 1675–1692.

5 F. Neese, *WIREs Comput. Mol. Sci.*, 2012, **2**, 73–78.

6 F. Neese, *WIREs Comput. Mol. Sci.*, 2022, **12**, e1606.

7 J. P. Perdew, K. Burke and M. Ernzerhof, *Phys. Rev. Lett.*, 1996, **77**, 3865–3868.

8 C. A. de Almeida, L. P. N. M. Pinto, H. F. Dos Santos and D. F. S. Paschoal, *J. Mol. Model.*, 2021, **27**, 322.

9 H. E. Gottlieb, V. Kotlyar and A. Nudelman, *J. Org. Chem.*, 1997, **62**, 7512–7515.

10 M. Van de Weert and L. Stella, *J. Mol. Struct.*, 2011, **998**, 144–150.

11 M. van de Weert, *J. Fluoresc.*, 2010, **20**, 625–629.

12 Methodology | Databases & Tools | Developmental Therapeutics Program (DTP), https://dtp.cancer.gov/databases_tools/docs/compare/compare_methodology.htm, (accessed February 27, 2023).

13 S. Sookai and O. Q. Munro, *ChemistryEurope*, 2023, **1**, e202300012.

14 S. Sookai and O. Q. Munro, *Dalton Trans.*, 2023, 52 14774-14789.

15 S. Sookai, M. L. Bracken and M. Nowakowska, *Molecules*, 2023, **28**, 7466.